NASA TM X-511

TECHNICAL MEMORANDUM

X-511

AERODYNAMIC CHARACTERISTICS OF A GROUP OF WINGED REENTRY VEHICLES AT MACH NUMBER 6.01 AT ANGLES OF ATTACK FROM 60° TO 120° AND -10° TO 30° ROLL AT 90° ANGLE OF ATTACK

By James G. Hondros and Theodore J. Goldberg

Langley Research Center
Langley Field, Va.

NATIONAL AERONAUTICS AND SPACE ADMINISTRATION
WASHINGTON June 1961

NATIONAL AERONAUTICS AND SPACE ADMINISTRATION

TECHNICAL MEMORANDUM X-511

AERODYNAMIC CHARACTERISTICS OF A GROUP OF WINGED REENTRY VEHICLES AT MACH NUMBER 6.01 AT ANGLES OF ATTACK FROM 60° TO 120° AND -10° TO 30° ROLL AT 90° ANGLE OF ATTACK*

By James G. Hondros and Theodore J. Goldberg

SUMMARY

An investigation of the effects of model geometry on the aerodynamic characteristics of a group of winged reentry vehicles has been conducted at a free-stream Mach number of 6.01 and tunnel Reynolds number of 7.6×10^6 per foot. Lateral and longitudinal forces and moments were measured on a strain-gage balance over an angle-of-attack range from 60° to 120° and a roll angle range from -10° to 30° at 90° angle of attack. The configurations consisted of 1 circular and 10 geometric variations of delta planform models having basically the same planform area with variations such as squared and rounded leading edges, sharp and rounded corners, leading and trailing-edge sweep angles, rounded or flat bottoms, and clipped wing tips.

The results of this investigation indicate that wing geometry had no noticeable effect on the lift coefficient or the lift-drag ratio for the flat-bottom models. All models could be trimmed and were laterally and longitudinally stable over the angle ranges of the investigation. Decreases in the drag coefficient were obtained with an increase in sweep angle over most of the angle-of-attack range except around 90°. Rounding the bottoms of the delta models reduced the normal-force and drag coefficients at all angles of attack with maximum reduction of about 9 percent for the unclipped model and 13 percent for the clipped model. Considerable increase in the slope of the body side-force-coefficient curve was obtained by this geometry change which resulted in a reduced lateral-range potential. In general, the magnitude of all force and moment coefficients, with exception of pitching-moment coefficient, remain about constant or increase with increasing Mach number up to 6.01. A modified Newtonian theory using a maximum pressure coefficient of 1.818 predicted very well the lift coefficient and the lift-drag ratio above 65° while the drag coefficient was overpredicted near 90° angle of attack and underpredicted near 60° angle of attack.

INTRODUCTION

Current interest in lifting manned reentry vehicles has initiated a general investigation by the National Aeronautics and Space Administration to provide aerodynamic data on configurations for use in vehicle design. Such problems as reentry heating, lateral and longitudinal range, and control capabilities are all dependent on the aerodynamic characteristics of the reentry vehicle.

Reentry vehicles which can provide lift and consequently have lift-drag ratios greater than zero permit pilot-controlled flight and selection of landing points whereas those which are not capable of producing lift re-enter in a ballistic path. One type of vehicle which produces lift is the winged vehicle. Winged vehicles may exercise two types of reentry manuevers. One is by employing the vehicle as a hypersonic glider flying at low angle-of-attack attitudes and by using wing aerodynamic lift to make a modulated or skip reentry. The second manuever is to have the vehicle enter the earth's atmosphere at a large angle of attack, thereby providing the high drag type of reentry which results in a lower total heat load to the vehicle, while maintaining some lift available for range control, and to alleviate high g-loads.

A knowledge of the longitudinal stability characteristics and trim capabilities of the vehicle is essential for the development of a workable design. In order to provide information with which to evaluate this type vehicle, the Langley Research Center has been engaged in a wind-tunnel program of generalized configurations covering the subsonic-, supersonic-, and hypersonic-speed ranges. Some results of the subsonic program can be seen in references 1 to 3, while some supersonic and hypersonic results are reported in references 4 to 6 and references 7 and 8, respectively.

The purpose of this investigation is to present the results of a program that has been designed to show the effects of model geometry on aerodynamic characteristics at high angles of attack. The configurations consisted of 1 circular and 10 geometric variations of delta planform models having basically the same planform area with variations such as leading-edge and trailing-edge sweep angles, rounded or flat bottoms, clipped wing tips, squared and rounded leading edges, and sharp and rounded corners. These same models have been tested at lower Mach numbers and are reported in reference 5.

This investigation was carried out in the Langley 20-inch Mach 6 tunnel at a Mach number of 6.01 and a Reynolds number of 7.6×10^6 per foot. The forces and moments were measured by means of a wire-strain-gage balance through an angle-of-attack range of 60° to 120° and an angle-of-roll range of -10° to 30° at an angle of attack of 90°.

SYMBOLS

The longitudinal and lateral forces and moments are referred to the body and stability axes as shown in figure 1 unless otherwise noted. The moment reference centers taken at the centroid of area are given in table I.

b	maximum span, in.
c	root chord, in.
C_A	axial-force coefficient, F_A/qS
C_D	drag coefficient, F_D/qS
C_L	lift coefficient, F_L/qS
C_l	rolling-moment coefficient, M_X/qSb
C_m	pitching-moment coefficient, M_Y/qSc
C_N	normal-force coefficient, F_N/qS
$C_{N,90^\circ}$	normal-force coefficient in roll at 90° angle of attack, $F_{N,90^\circ}/qS$
C_{p_b}	base-pressure coefficient, $\frac{p_b - p}{q}$
C_p	pressure coefficient, $\frac{p_{t,2} - p}{q}$
C_Y	side-force coefficient, F_Y/qS
d	diameter of circle cut from sphere, in.
F_D	drag force, lb
F_A	axial force, lb
F_N	normal force, lb

$F_{N,90^o}$	normal force in roll at 90° angle of attack, lb
F_Y	side force, lb
F_L	lift force, lb
L/D	lift-drag ratio, F_L/F_D
M	free-stream Mach number
M_X	rolling moment, in-lb
M_Y	pitching moment, in-lb
p	free-stream static pressure, lb/sq in. abs
p_b	base pressure, lb/sq in. abs
$p_{t,2}$	total pressure behind normal shock, lb/sq in. abs
p_0	stagnation pressure, lb/sq in. abs
q	free-stream dynamic pressure, $\frac{\gamma p M^2}{2}$, lb/sq in.
r	radius of sphere, in.
S	planform area, sq in.
x_{cp}	longitudinal center of pressure, percent of root chord
y_{cp}	lateral center of pressure, percent of maximum span
X,Y,Z	body axes of coordinate systems unless otherwise designated
α	angle of attack, deg
α_{trim}	trim angle of attack for $C_m = 0$, deg
β	angle of sideslip, deg
γ	ratio of specific heats of air, (1.4)

Λ	sweep angle of the wing leading edge, deg
ϕ	angle of roll, deg

Subscripts:

s	stability axes
w	wind axis
max	maximum

APPARATUS AND TEST METHODS

The tests were conducted at a Reynolds number of 7.6×10^6 per foot in the Langley 20-inch Mach 6 tunnel. The tunnel, which has been described in reference 9, is a blowdown to atmosphere type capable of operation at a maximum stagnation pressure of 580 lb/sq in. and a maximum stagnation temperature of 600° F. The air is dried by an activated alumina dryer designed to provide a dewpoint temperature of -40° F at 600 lb/sq in.

The models were supported in the tunnel by the "goose-neck" support system shown in figures 2 and 3 which moved the model in the horizontal plane. This support system limited the angle-of-attack range from -10° to 30° when using a straight sting. Therefore, in order to test the models over the desired 60° to 120° angle-of-attack range, it was necessary to rotate the model 180° about the balance. The models were mounted with the upper surface normal to the center line of the balance (as shown in fig. 3). This required a sting extension between the model and the balance having a small diameter (0.188 inch) in order to minimize the effects of pressure interference on the rear of the model. The balance and sting extension were calibrated as a unit representing test conditions to eliminate errors due to balance and sting deflections. The angle of attack was measured mechanically by a counter geared to the vertical shaft of the support system.

Model forces were measured with a water-cooled, 3-component wire-strain-gage balance with components of normal force, axial force, and pitching moment. A wind shield covering the balance and sting extension was employed to prevent the measurement of extraneous loads. A copper ring was inserted in the wind shield at the closest point to the model and wired to complete an electric circuit if contacted by the sting extension to indicate fouling.

Two 0.090 O.D. tubes located about 1/8 inch from each side of the sting were used to measure the base pressures in the chordwise and spanwise planes for angles of attack and roll, respectively. The two base pressures and the tunnel stagnation pressure were measured with 0 to 1.0 lb/sq in. abs and 0 to 600 lb/sq in. pressure transducers, respectively.

MODELS

The models used in this investigation are the same as those reported in reference 5. The configurations consisted of 1 circular planform wing and 10 geometric variations of a delta planform wing. All delta planform models had a fuselage which consisted of a semi-cone cylinder above a 1/8-inch flat plate mounted on the upper surface. Changes in the model parameters consisted of rounding corners and leading edges, varying leading- and trailing-edge sweep angle, rounding the flat bottoms and clipping wing tips. A photograph of these models is shown in figure 4. Model dimensions are given in tables I and II.

DATA REDUCTION AND ACCURACY

All force and moment coefficients and centers of pressure were based upon the individual model planform area and the root chord or maximum span. Longitudinal and lateral centers of pressure were computed on the assumption that body axial force and side force acted through the model moment center. Moment transfers were made from the balance moment center to the model moment center by standard transfer equations.

The maximum uncertainties of the force and moment coefficients of the individual test points in the balance system are as follows:

C_N	±0.012
C_A	±0.020
C_Y	±0.012
C_m	±0.011
C_l	±0.015

Tunnel stagnation pressure was 400 lb/sq in. abs with a variation of ±3 lb/sq in. abs, while base-pressure measurements are believed accurate to ±0.0025 lb/sq in. abs. The tunnel Mach number was 6.01

with a possible variation of ±0.02. Model alinement and angle-of-attack measurements are each accurate to ±30 minutes.

RESULTS AND DISCUSSION

The basic aerodynamic characteristics of the 11 models with a nearly-constant planform area are presented in figure 5. The data shown have not been corrected for measured base pressures. These base pressures and the base-pressure coefficients are shown in figures 6 and 7. A value from the faired curve through all the base-pressure-coefficient points plotted in figure 7 would yield a variation of less than 1 percent in the normal-force coefficient of any model at any angle of attack. It should be noted that these base pressures were only measured near the sting and therefore are not necessarily indicative of the pressures over the rest of the wing.

Typical schlieren photographs of some of the models tested at 90° angle of attack are presented in figure 8. The photographs were taken in the angle-of-attack and angle-of-roll positions to show the changes in the chordwise- and spanwise-shock location and shock shape indicating pressure-relieving effects due to changes in model geometry.

The results of figure 5 have been replotted in figures 9 to 15 to facilitate the detailed comparisons of the effects of individual geometric changes on the basic aerodynamic characteristics. The assumption that the axial force acted through the model moment center made for the computation of longitudinal center of pressure can be seen to be valid within the accuracy of the data by comparing the longitudinal trim points found from the pitching-moment-coefficient curves and the longitudinal center-of-pressure curves together with the location of the moment reference center (c.g.) in figures 9 to 15.

Effects of Rounding Corners and Leading Edges

The effects on the basic aerodynamic characteristics of rounding the corners and edges of a delta-wing model are presented in figure 9. The reduction in normal-force coefficient for model 2 increased with increasing angle of attack up to about 85° and thereafter remained nearly constant while the reduction in drag coefficient for model 2 reached a maximum at about 90° angle of attack. At 90° angle of attack the value of 1.67 for $C_{D,max}$ (or $C_{N,max}$) for model 2 was only about $2\frac{1}{2}$ percent lower than model 1 (fig. 9(a)) indicating little pressure

relief due to rounding corners and leading edges. The lift coefficients and the lift-drag ratios were essentially unaffected by these geometric changes.

Rounding the corners and edges apparently increased the stable pitching-moment range from about 73° through 120° to 60° through 120° angle of attack and moved the trim point from an angle of attack of about 92° to 62° (fig. 9(a)). The rolling-moment-coefficient curves in figure 9(b) were about the same for both models and show stable rolling-moment coefficients over the range of roll angles tested at 90° angle of attack.

Effect of Leading-Edge Sweep Angle

The effects of leading-edge sweep angle on the aerodynamic characteristics of round corner delta wings can be seen in figure 10 by comparing models 8, 2, and 6 with sweep angles of 55°, 65°, and 75°, respectively. At lower angles of attack, references 10 and 11 have shown that increasing leading-edge sweep angle decreases the drag and normal-force coefficients. Reference 5 indicates that as the angle of attack increases the effect of leading-edge sweep on C_D and C_N diminishes until at 90° the drag coefficient, which is equal to the normal-force coefficient at 90°, becomes independent of the leading-edge sweep angle at Mach numbers of 2.38 and 2.99. However, at a Mach number of 4.00 the values of C_D and C_N for the 55° swept wing remained higher at 90° angle of attack than those for the other models which had equal values of C_D. The results of the present investigation at Mach number of 6.01 shown in figure 10(a) agree with those of reference 5 at Mach number of 4.00. This difference in drag coefficient at 90° angle of attack, though small, might indicate that at Mach numbers above 4.00 sweep angles less than 65° afford less pressure relief thus resulting in higher values of C_D and C_N while for sweep angles of 65° and above no effect on C_D and C_N at 90° angle of attack is found.

Sweep angle had no effect on the lift coefficient and the lift-drag ratio except possibly at 60° angle of attack where the 55° swept model had slightly higher values due to the large increase in the normal-force coefficient. However, the larger increase in C_N at 120° angle of attack does not increase the lift coefficient and the lift-drag ratio due to the negative increase in C_A. There was very little effect on the stable pitching-moment coefficients at all angles of attack except at around 60° and 120° where the 55° swept model had larger pitching moments. The 55° swept wing had a trim point which occurred at about 67° angle of attack whereas the other two models trimmed around

62° angle of attack. In general, the negative slope of the rolling-moment-coefficient curve (fig. 10(b)) increased with a decrease in sweep angle.

Effect of Clipping Wing Tips

The effects on the aerodynamic characteristics of clipping the tips of a 75° swept, flat-bottom model and 65° swept, flat-bottom and rounded-bottom models are presented in figure 11. It is apparent that practically all force and moment coefficients remained unchanged. Only the pitching-moment coefficients of the 65° swept, rounded-bottom model (fig. 11(c)) and the 75° swept, flat-bottom model (fig. 11(e)) were slightly increased by clipping the wing tips, and only the side-force coefficient was decreased by clipping the wing tips on the 65° swept, flat- and rounded-bottom models as shown in figures 11(b) and 11(d), respectively.

Clipping the wing tips on the flat-bottom models apparently slightly increased the longitudinal stability range to include the 60° to 65° angle-of-attack region (figs. 11(a) and 11(e)) and allowed the 65° and 75° swept models to be trimmed at about 67° and 82° angle of attack, respectively. Both round-bottom models were longitudinally stable (fig. 11(c)) over the angle-of-attack range with the α_{trim} moved from about 67° to 82° by clipping the wing tips.

It is evident from the negative slopes of the rolling-moment coefficient curves in figures 11(b), 11(d), and 11(f) that all models were laterally stable through the angle-of-roll range at 90° angle of attack.

Effects of Trailing-Edge Sweep

The effects of trailing-edge sweep on the aerodynamic characteristics of a clipped delta wing are presented in figure 12. Although there was no effect on the lift-drag ratio or the lift coefficient, sweeping the trailing edge 43° inward (model 5) reduced the normal-force and drag coefficients in the 60° to 90° angle-of-attack range whereas sweeping the trailing edge 32° outward (model 4) reduced these coefficients in the 90° to 120° angle-of-attack region.

The pitching-moment coefficient (fig. 12(a)) was only slightly increased with outward sweep of the trailing edge (model 4) and the trim point moved from about 67° to 81° angle of attack. Sweeping the trailing edge inward (model 5) produced a much larger increase in the pitching-moment coefficient, especially at the lower angles of attack, and moved the α_{trim} further back to about 96°. In addition, sweeping

the trailing edge inward (model 5) results in greater stability as indicated by the increased negative slope of the C_m curve (fig. 12(a)). The increased pitching-moment coefficient combined with the decrease in normal-force coefficient at the lower angles of attack indicate a much greater pressure relief at the rear of the inward-swept trailing-edge model (model 5).

The 43° inward-swept trailing-edge model (model 5) had a larger shift in the center of pressure (about 15-percent root chord from 60° to 120° angle of attack as compared to about a 6-percent shift for the other models).

All three models were laterally, as well as longitudinally, stable as seen by the negative slope of the rolling-moment-coefficient curve (fig. 12(b)). The greatest effect on the side-force coefficient occurred at 30° roll angle where the inward-swept trailing-edge model produced the largest value of about -0.13 and the unswept trailing-edge model had the smallest side-force coefficient of about -0.08. One possible explanation of the increase in side-force coefficient may be due to flow impingement on the inner surface of the inward-swept trailing edge at this high roll angle.

Effects of Rounding Bottom

The effects of rounding the bottom of a flat-plate delta-wing model on the lateral and longitudinal aerodynamic characteristics are shown in figure 13. Rounding the bottom on the unclipped delta-wing model (model 9) decreased the magnitude of the lift coefficient by an average of 8 percent at all angles of attack (fig. 13(a)). Rounding the bottom of the clipped model (model 10) had no effect on the lift coefficient up to 90° angle of attack, but the values of the coefficients decreased with increasing angle of attack above 90° by as much as 15 percent at 120° angle of attack (fig. 13(c)). The lift-drag ratio for the unclipped model (model 5, fig. 13(a)) appeared to be unaffected whereas the ratio for the clipped model (model 10, fig. 13(c)) was reduced about 10 percent at around 120° angle of attack by rounding the bottom. The normal-force and drag coefficients were reduced at all angles of attack of the investigation due to the pressure relief afforded by the curvature on the lower surface of the rounded-bottom wings. These maximum reductions of about 9 percent and 13 percent for the unclipped and clipped models, respectively, occurred at 60° angle of attack (figs. 13(a) and 13(c)). The maximum values of the normal- and drag-force coefficients of 1.67, occurring at 90° angle of attack, were reduced about 3.5 percent (figs. 13(a) and 13(c)).

Rounding the bottom of the unclipped model only affected the pitching-moment coefficients at about 60° and 120° angle of attack (fig. 13(a)). However, this permitted the model to be trimmed at an α_{trim} of about 67° whereas the flat-bottom model was trimmed at about 62°. For the clipped-tip models (models 3 and 10) the values of the pitching-moment coefficients were increased (fig. 13(c)) and the trim point was shifted from an α_{trim} of about 70° to 82° by rounding the bottom. All models in figure 13 were longitudinally stable at all angles of attack.

The rolling-moment coefficients were not significantly altered by rounding the bottoms of the clipped- or unclipped-delta-wing models which were laterally stable over the entire roll range tested at 90° angle of attack as seen in figures 13(b) and 13(d). Apparently rounding the bottom in the longitudinal plane offsets any effect on the rolling-moment coefficient that might be expected from rounding the bottom in the lateral plane.

A considerable increase in the negative slopes of the side-force-coefficient curves (figs. 13(b) and 13(d)) resulted from rounding the bottoms of the clipped and unclipped models. This increase in side-force coefficient would tend to indicate an extension of the lateral-range capabilities of the rounded-bottom models. However, the large decrease of normal force in roll seen in figures 13(b) and 13(d), from 5 percent at 0° roll angle to 15 percent at 30° roll angle at 90° angle of attack, outweighs the increase in side-force coefficient thereby resulting in a net decrease of the lateral-range potential. This potential can be seen in figure 14 which is a plot of the variation of side-force coefficient with drag coefficient on the wind axes at 90° angle of attack over the range of roll angles tested for the flat- and rounded-bottom models. For a constant drag coefficient, there is a decrease in side-force coefficient for the rounded-bottom models which would yield a smaller lateral range for a 90° reentry attitude.

Comparison of Round-Bottom Circular and Delta Planform Wings

The effect on the aerodynamic characteristics of changing planform from a rounded-bottom delta wing to a rounded-bottom circular wing is shown in figure 15. It should be pointed out that a direct comparison cannot be made since the bottom curvature is not the same for both models. The circular planform wing has a curvature equivalent to that of a sphere with a 7.23-inch radius (see table I) whereas the delta planform wing has a chordwise curvature of approximately a 6-inch radius and a spanwise

curvature at the trailing edge of approximately a 4-inch radius. (See table II.) However, some qualitative results can still be pointed out.

The circular planform model produced a higher drag coefficient than the delta planform model at all angles of attack by an average of about 9 percent. This may be attributed to the fact that it has less curvature (a larger radius) on the bottom than does the delta planform wing and thereby would be expected to afford less pressure relief. As can be seen in figure 5(e), the circular planform model with the rounded bottom even produced a higher drag coefficient than the flat-bottom delta planform models for angles of attack of 65° to 115°. It is reasonable to assume that the drag coefficient would be still higher for a flat-bottom circular planform wing. This is contrary to the results presented in reference 7 which show no effect on C_D by changing from a flat-bottom delta to a flat-bottom circular planform model.

Changing from a delta to a circular planform model increased the magnitude of the lift coefficients over most of the angle-of-attack range (fig. 15) but the lift-drag ratio remained unchanged, due to the aforementioned increase in drag coefficient, except at 120° where the L/D was increased by as much as 20 percent. This higher value of L/D is obviously caused by a larger increase in the magnitude of C_L together with the smaller increase in C_D. The circular planform wing gave higher values of pitching-moment coefficient and remained longitudinally stable over the angle-of-attack range.

Both models were laterally stable throughout the roll range with the circular planform model having only slightly higher values of rolling-moment coefficients. The increase in normal-force coefficient in roll from 7.5 to 18.5 percent apparently more than offsets the decrease in the slope of the side-force-coefficient curve (fig. 15(b)) thereby resulting in greater lateral-range potential for the circular model as seen in figure 14.

Comparison Between Predicted and Experimental Results

The lift and drag characteristics obtained from the modified Newtonian theory $(C_{p,max} = 1.818)$ are compared with the experimental values for all the flat-bottom models tested in figure 16. It can be seen that the predicted lift coefficients agree very well with the measured values for angles of attack above 65°. This was also found to be true in reference 7 where modified Newtonian gave good predictions above 65° but below 65° angle of attack unmodified Newtonian theory $(C_{p,max} = 2.0)$ resulted in better predictions, although both methods underpredicted for angles of attack below 55°. For the

angle-of-attack range of the investigation the modified Newtonian theory ($C_{p,max} = 1.818$) fairly well predicts the drag coefficients of these flat-bottom wings for the 60° to 75° and 105° to 120° ranges but overpredicts in the range of 75° to 105° as pointed out in reference 12 and found in reference 7. Predicted modified Newtonian values of lift-drag ratio are in excellent agreement with the experimental results at all angles of attack of the investigation.

Mach Number Effects

The effects of Mach number on some of the aerodynamic characteristics of these models are presented in figure 17. The data taken from reference 5 at Mach number of 2.38, 2.99, and 4.00 and the data taken at Mach number 6.01 in this report have all be adjusted for a base-pressure coefficient of $-1/M^2$ for this comparison.

The points at lower Mach numbers, 2.38 specifically, indicate higher drag coefficients and normal-force coefficients in roll primarily due to the method of base pressure adjustment to a value of $-1/M^2$ which is considerably less than that obtained in reference 13 on cylindrical bodies.

The curves in figure 17 indicate a drag coefficient increase with increasing Mach number. A maximum increase of about 16 percent was attained on the rounded-bottom, circular planform wing (fig. 17(f)). In general, the lift coefficient and the lift-drag ratio increase with Mach number with a maximum increase of about 22 percent on the rounded-bottom, unclipped delta model (fig. 17(d)).

The pitching-moment-coefficient curves of figure 17 show several shapes so that a general statement concerning them cannot be made; however, there are certain groups of models that seem to show the same general characteristics. It is interesting to note that the only model which showed no variation of pitching-moment coefficient with Mach number was model 3. (See fig. 17(h).) In most cases (models 1, 4, 5, 9, 10, and 11) the pitching-moment-coefficient curves of figure 17 tend to give a fan-shaped divergent series of curves with angle of attack; that is, in the lower range from 60° to 90° the slope is generally positive and in the 90° to 120° range the slope is generally negative. Models 6 and 8 show a general trend of negative slope with Mach number while model 7 has a tendency to indicate negative slopes up to about a Mach number of 4.5 and then reverses slope up to a Mach number of 6.01. The greatest variation in the magnitude of the pitching-moment coefficient is about 0.125 occurring at 60° angle of attack on the inward-swept trailing-edge model (model 5).

Lateral data (side-force, normal-force in roll, and rolling-moment coefficients) for models 2, 3, 6, 7, and 10, in general, tend to increase in magnitude or remain constant for roll angles from 0° to 30° with increasing Mach number. (See figs. 17(g) to 17(k).) The 75° swept, clipped-tip model (model 7, fig. 17(j)) gave the maximum increases in magnitude of normal-force coefficient in roll and side-force coefficient of 0.09 and 0.12, respectively, at 30° roll angle. Rolling-moment coefficient had a maximum change in magnitude of 0.03 occurring on models 3, 6, and 7 as shown in figures 17(h), 17(i), and 17(j), respectively.

The data shown in figure 17 can be summarized, in general, by stating that the magnitude of all force and moment coefficients, with the exception of pitching moment, remain about constant or increase with increasing Mach number to 6.01.

CONCLUSIONS

The results of an investigation of a group of winged reentry vehicles at a Mach number of 6.01 and comparisons with results at lower supersonic Mach numbers and a modified Newtonian theory at angles of attack from 60° to 120° and at angles of roll from -10° to 30° at 90° angle of attack indicate the following conclusions:

1. Wing geometry had no noticeable effect on the lift coefficient or the lift-drag ratio for all flat-bottom models.

2. All models could be trimmed and were laterally and longitudinally stable over the angle range of the investigation.

3. For round corner delta wings an increase in sweep angle decreased the drag coefficient over most of the angle-of-attack range except near 90° where the 55° swept model had a higher drag coefficient than the 65° and 75° swept models which were equal. In general, a decrease in sweep angle increased the slope of the rolling-moment-coefficient curve.

4. Increases in pitching moment were obtained by clipping the wing tips of the delta models. This allowed the trim point to be moved to higher angles of attack.

5. Rounding the bottoms of the delta models reduced the drag coefficients at all angles of attack with maximum reductions of about 9 percent for the unclipped model and 13 percent for the clipped model and considerably increased the slope of the side-force-coefficient curve which resulted in a reduced lateral-range potential.

6. In general, the magnitude of all force and moment coefficients, with the exception of pitching-moment coefficient, remain about constant or increase with increasing Mach number up to 6.01.

7. Modified Newtonian theory (maximum pressure coefficient of 1.818) predicted very well the lift coefficient and the lift-drag ratio above 65° whereas the drag coefficient was overpredicted near 90° angle of attack and underpredicted near 60° angle of attack.

Langley Research Center,
National Aeronautics and Space Administration,
Langley Field, Va., January 13, 1961.

REFERENCES

1. Spencer, Bernard, Jr.: High-Subsonic-Speed Investigation of the Static Longitudinal Aerodynamic Characteristics of Several Delta-Wing Configurations for Angles of Attack from 0° to 90°. NASA TM X-168, 1959.

2. Fournier, Paul G.: Wind-Tunnel Investigation at High Subsonic Speed of the Static Longitudinal Stability Characteristics of a Winged Reentry Vehicle Having a Large Negatively Deflected Flap-Type Control Surface. NASA TM X-179, 1959.

3. Paulson, John W.: Low-Speed Static Stability Characteristics of Two Configurations Suitable for Lifting Reentry From Satellite Orbit. NASA MEMO 10-22-58L, 1958.

4. Foster, Gerald V.: Exploratory Investigation at Mach Number of 2.01 of the Longitudinal Stability and Control Characteristics of a Winged Reentry Configuration. NASA TM X-178, 1959.

5. Smith, Fred M., and Nichols, Frank H., Jr.: A Wind-Tunnel Investigation of the Aerodynamic Characteristics of a Generalized Series of Winged Reentry Configurations at Angles of Attack to 180° at Mach Numbers of 2.38, 2.99, and 4.00. NASA TM X-512, 1961.

6. Dugan, Duane W.: Estimation of Static Longitudinal Stability of Aircraft Configurations at High Mach Numbers and at Angles of Attack Between 0° and ±180°. NASA MEMO 1-17-59A, 1959.

7. Penland, Jim A., and Armstrong, William O.: Static Longitudinal Aerodynamic Characteristics of Several Wing and Blunt-Body Shapes Applicable for Use as Reentry Configurations at a Mach Number of 6.8 and Angles of Attack up to 90°. NASA TM X-65, 1959.

8. Close, William H.: Hypersonic Longitudinal Trim, Stability, and Control Characteristics of a Delta-Wing Configuration at High Angles of Attack. NASA TM X-240, 1960.

9. Ashby, George C., Jr., and Fitzgerald, Paul E., Jr.: Longitudinal Stability and Control Characteristics of Missile Configurations Having Several Highly Swept Cruciform Fins and a Number of Trailing-Edge and Fin-Tip Controls at Mach Numbers from 2.21 to 6.01. NASA TM X-335, 1960.

10. Gallagher, James J., and Mueller, James N.: An Investigation of the Maximum Lift of Wings at Supersonic Speeds. NACA Rep. 1227, 1955. (Supersedes NACA RM L7J10.)

11. Kaattari, George E.: Pressure Distributions on Triangular and Rectangular Wings to High Angles of Attack - Mach Numbers 2.46 and 3.36. NACA RM A54J12, 1955.

12. Penland, Jim A., and Armstrong, William O.: Preliminary Aerodynamic Data Pertinent to Manned Satellite Reentry Configurations. NACA RM L58E13a, 1958.

13. Love, Eugene S.: Base Pressure at Supersonic Speeds on Two-Dimensional Airfoils and on Bodies of Revolution With and Without Fins Having Turbulent Boundary Layers. NACA TN 3819, 1957. (Supersedes NACA RM L53C02.)

TABLE I.- GEOMETRIC CHARACTERISTICS OF MODELS

[The planform radii of all models except models 1 and 11 are 0.28 inch]

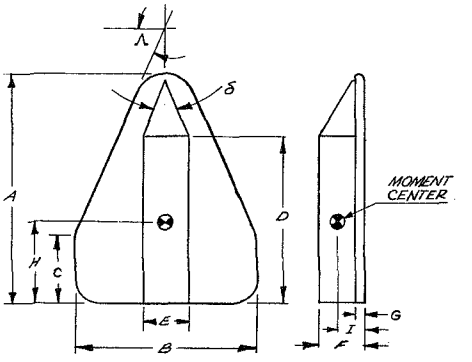

Model	A, in.	B, in.	C, in.	D, in.	E, in.	F, in.	G, in.	H, in.	I, in.	Λ, deg	δ, deg	Area, sq in.
1	2.92	2.72	0	2.24	0.500	0.466	0.120	0.973	0.269	65	40	3.97
2	2.61	2.48	0	1.88	.500	.462	.119	1.020	.269	65	40	4.00
3	2.67	2.18	.745	1.94	.500	.462	.119	1.084	.269	65	40	4.06
4	2.91	2.05	.569	2.17	.500	.463	.119	1.271	.269	65	40	4.06
5	2.82	2.29	.760	2.09	.500	.459	.118	1.228	.269	65	40	3.94
6	3.14	1.96	0	2.40	.500	.464	.119	1.280	.269	75	40	4.00
7	3.25	1.65	1.00	2.47	.500	.461	.119	1.347	.269	75	40	3.96
8	2.21	2.92	0	1.44	.500	.463	.119	.850	.269	55	40	3.98
9	2.63	2.48	0	1.88	.500	.537	.164	1.064	.269	65	40	4.12
10	2.74	2.16	.77	1.97	.500	.525	.155	1.107	.269	65	40	4.16
11	Circle of 2.256 diameter cut from sphere with 7.232-in. radius											4.00

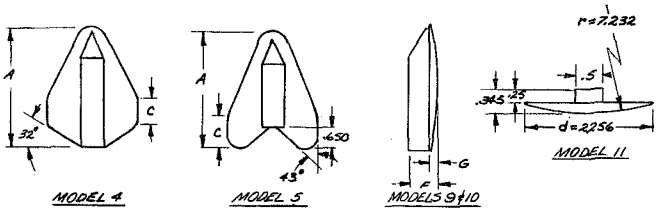

TABLE II.- COORDINATES OF CONTOURED WINGS

[All dimensions are in inches]

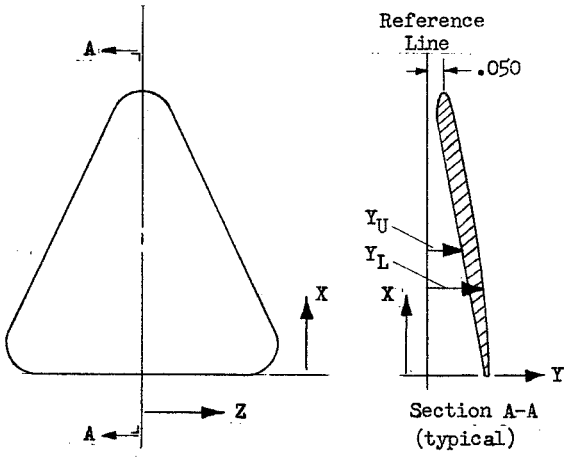

(a) Delta planform (model 9)

Z = 0			Z = ±.400			Z = ±.800			Z = ± 1.240		
X	Y_U	Y_L	X	Y_U	Y_L	X	Y_U	Y_L	X	Y_U	Y_L
0	.265	.296	0	.244	.275	0	.175	.206	0	.050	.081
0.200	.243	.313	0.200	.218	.293	0.200	.150	.220	.200	.045	.083
0.400	.223	.328	0.400	.195	.300	0.400	.128	.220	.343	.050	.050
0.600	.200	.335	0.600	.173	.303	0.600	.105	.205			
0.800	.178	.338	0.800	.150	.298	0.800	.080	.180			
1.000	.155	.330	1.000	.128	.285	1.000	.055	.140			
1.200	.135	.323	1.200	.105	.265	1.200	.033	.088			
1.400	.115	.305	1.400	.083	.238	1.287	.050	.050			
1.600	.093	.280	1.600	.060	.200						
1.800	.070	.253	1.800	.035	.158						
2.000	.050	.218	2.000	.018	.108						
2.200	.030	.175	2.145	.050	.050						
2.400	.015	.125									
2.615	.050	.050									

(b) Clipped delta planform (model 10)

Z = 0			Z = ±.324			Z = ±.648			Z = ± 1.080		
X	Y_U	Y_L	X	Y_U	Y_L	X	Y_U	Y_L	X	Y_U	Y_L
0	.240	.271	0	.223	.254	0	.173	.204	0	.050	.081
0.200	.223	.288	0.200	.205	.273	0.200	.155	.220	.200	.045	.105
0.400	.205	.300	0.400	.185	.283	0.400	.138	.228	.400	.040	.105
0.600	.185	.308	0.600	.168	.288	0.600	.118	.225	.600	.035	.088
0.800	.165	.310	0.800	.148	.285	0.800	.098	.215	.770	.050	.050
1.000	.145	.305	1.000	.128	.278	1.000	.078	.195			
1.200	.128	.300	1.200	.108	.268	1.200	.058	.170			
1.400	.108	.288	1.400	.088	.250	1.400	.038	.135			
1.600	.090	.270	1.600	.068	.225	1.600	.028	.093			
1.800	.073	.248	1.800	.048	.148	1.697	.050	.050			
2.000	.053	.218	2.000	.028	.163						
2.200	.033	.185	2.000	.013	.120						
2.400	.013	.145	2.39	.050	.050						
2.600	.013	.103									
2.700	.050	.050									

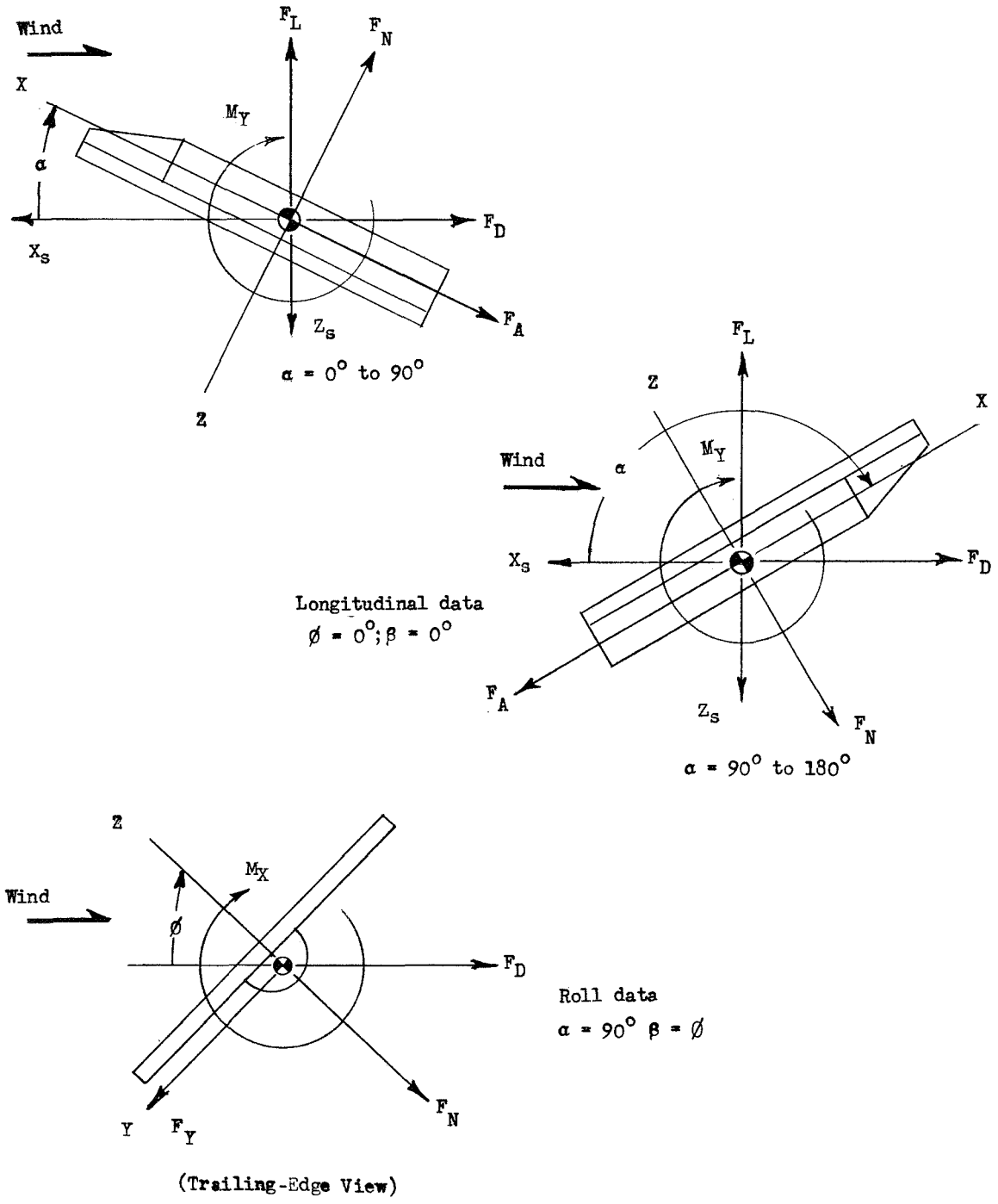

Figure 1.- Longitudinal and lateral axes system showing angles, forces, and moments.

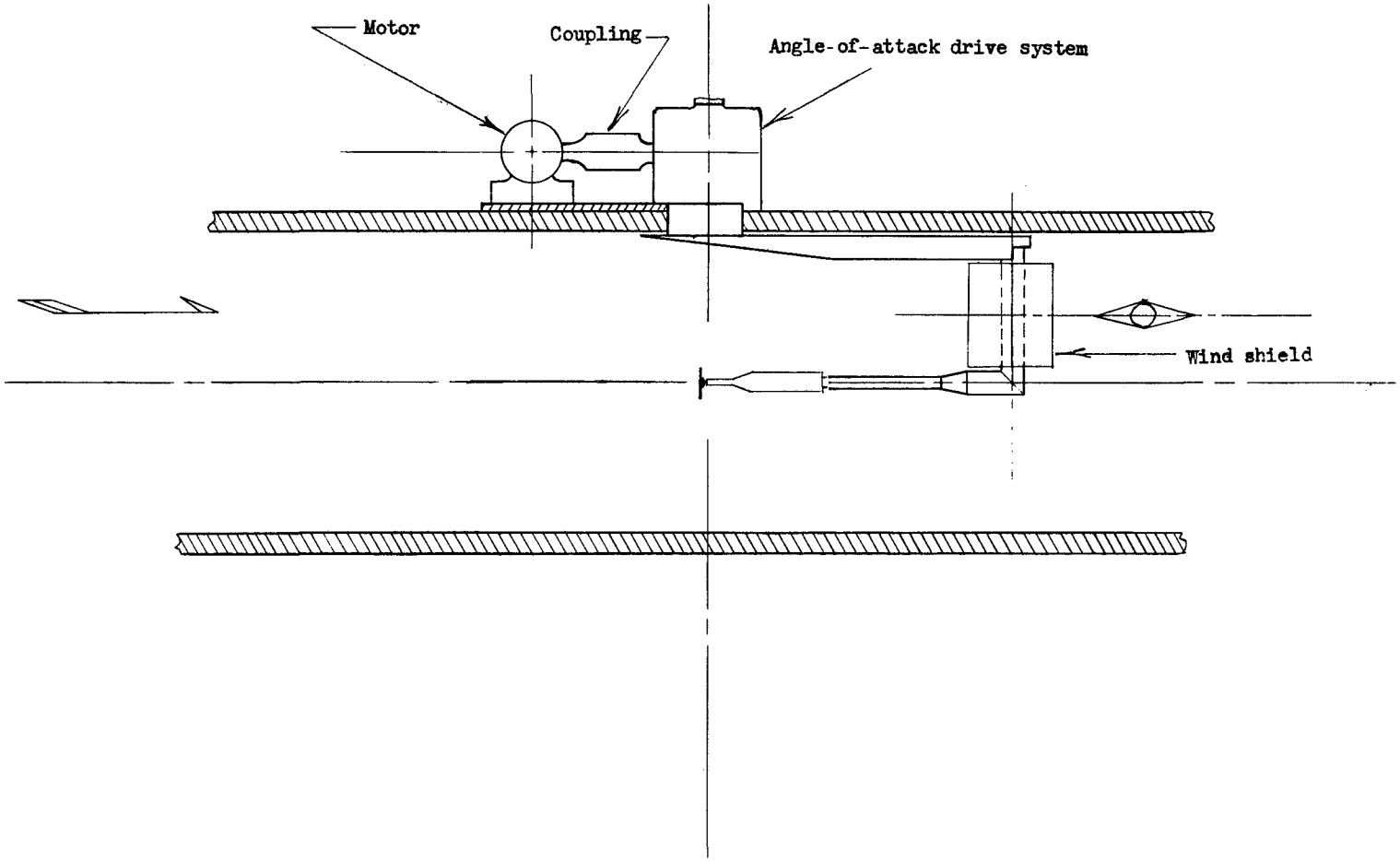

Figure 2.- Schematic diagram of model-support system.

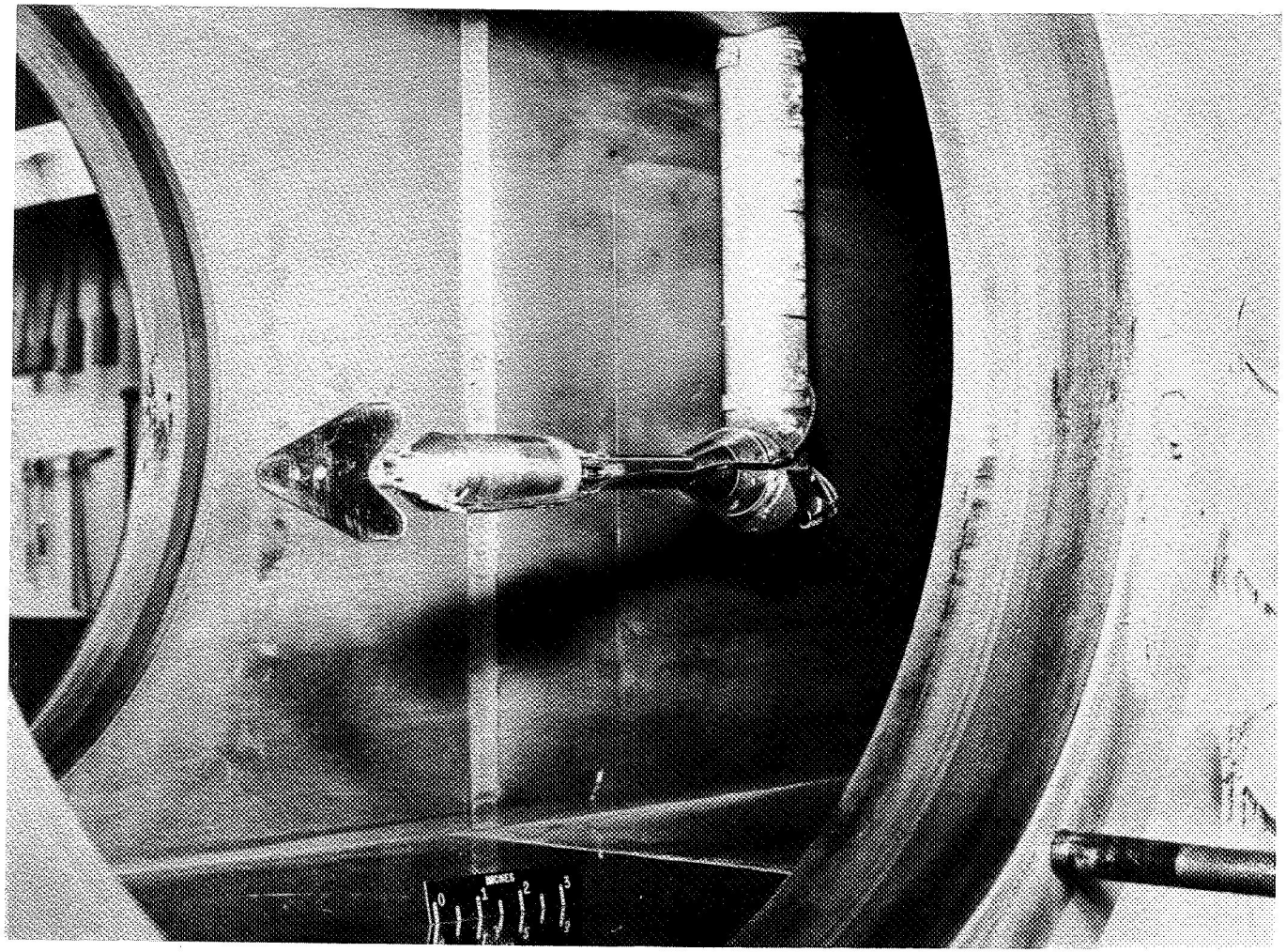

L-60-1677

Figure 3.- Photograph of model-support system with model and balance mounted in the Langley 20-inch Mach 6 tunnel.

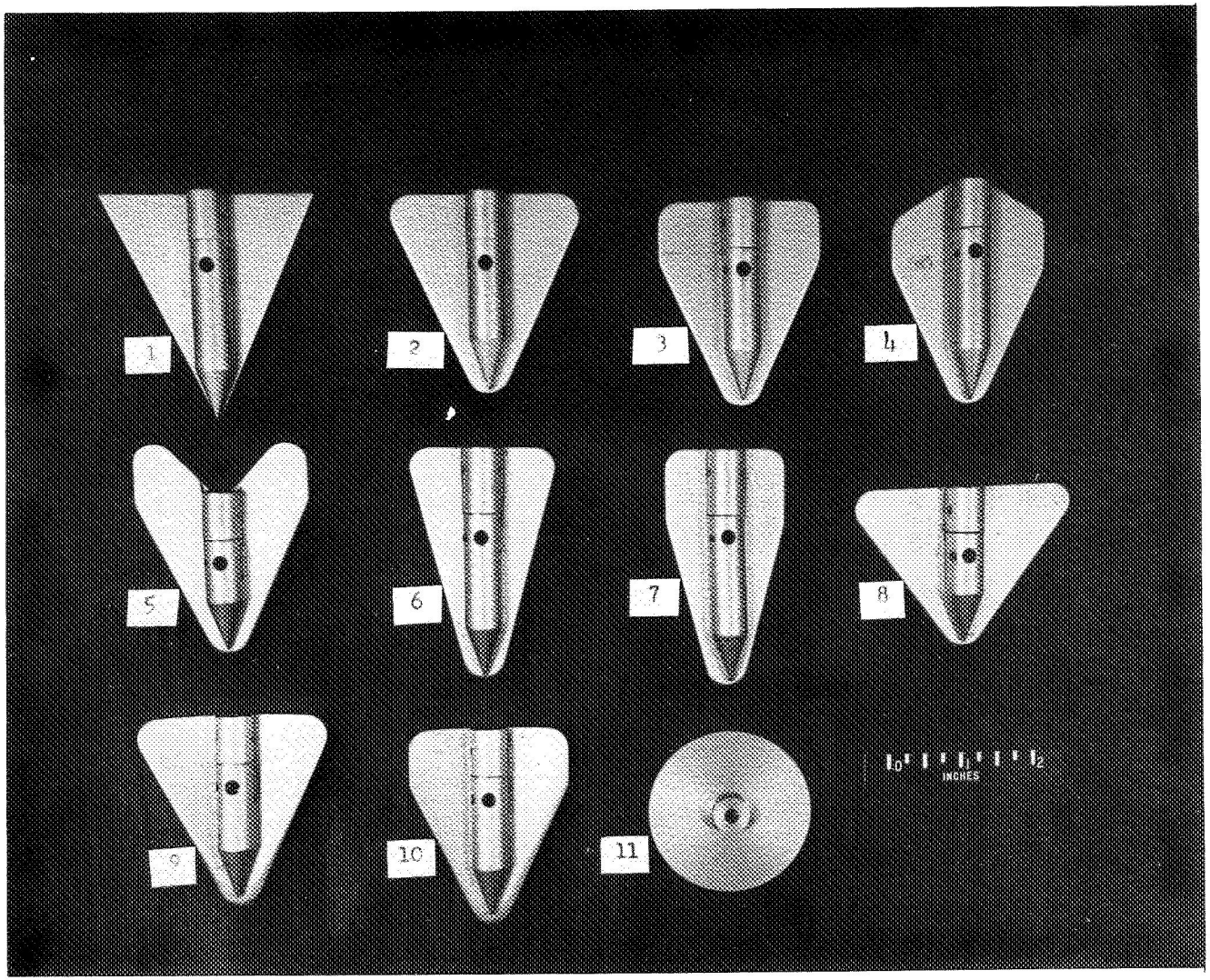

Figure 4.- Photograph of winged reentry models. L-60-6459.1

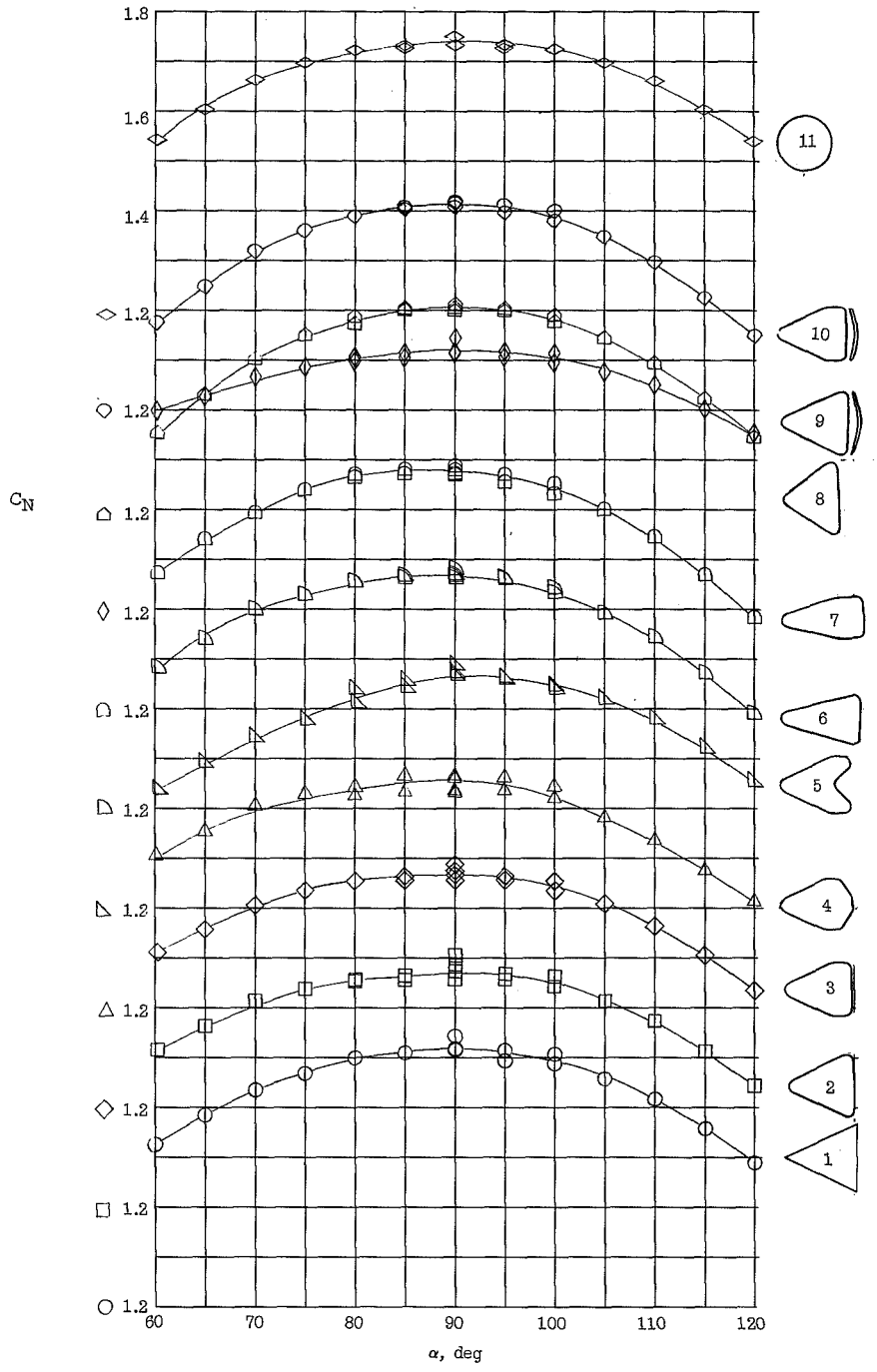

(a) Variation of normal-force coefficient with angle of attack.

Figure 5.- Basic aerodynamic characteristics of the 11 winged reentry models.

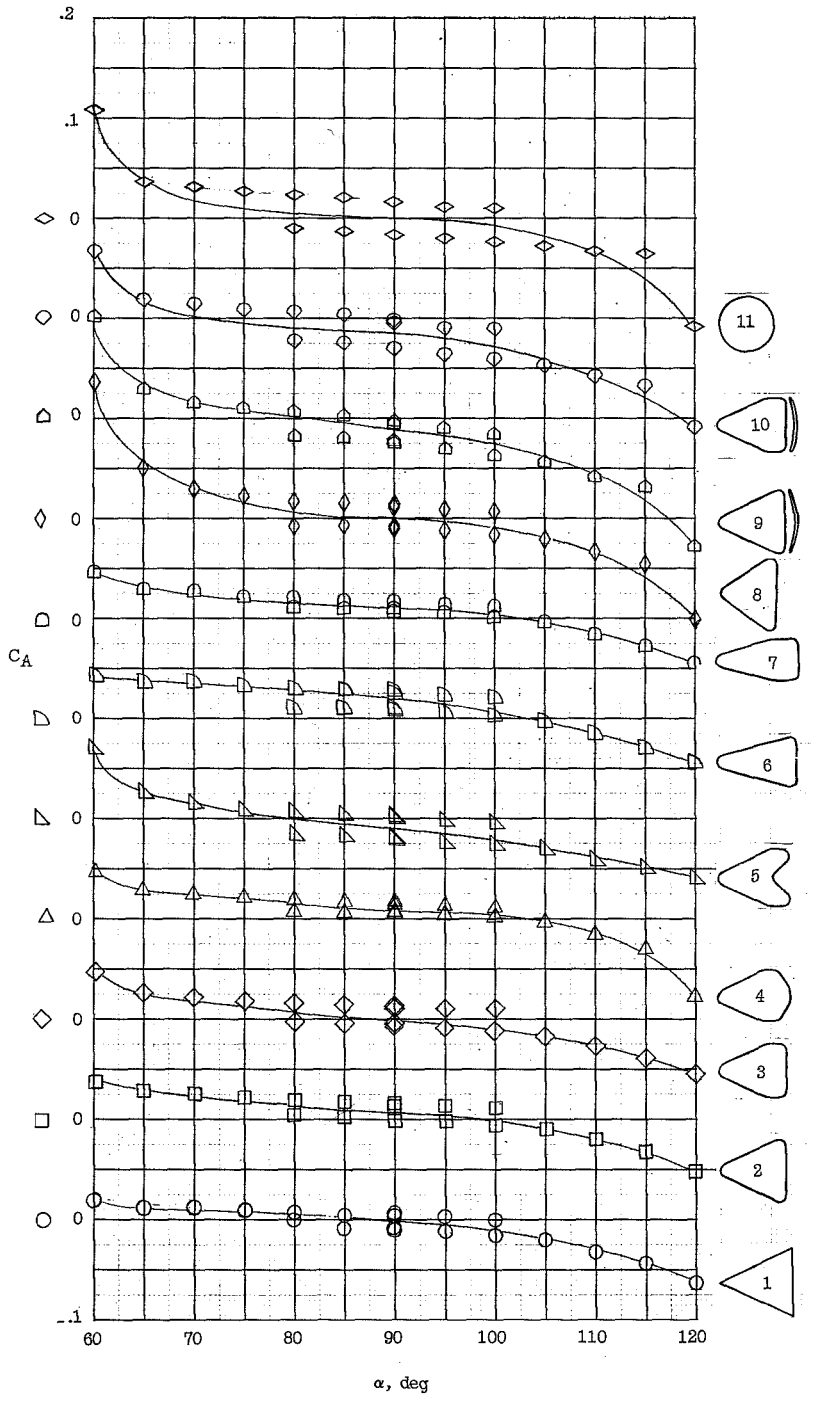

(b) Variation of axial-force coefficient with angle of attack.

Figure 5.- Continued.

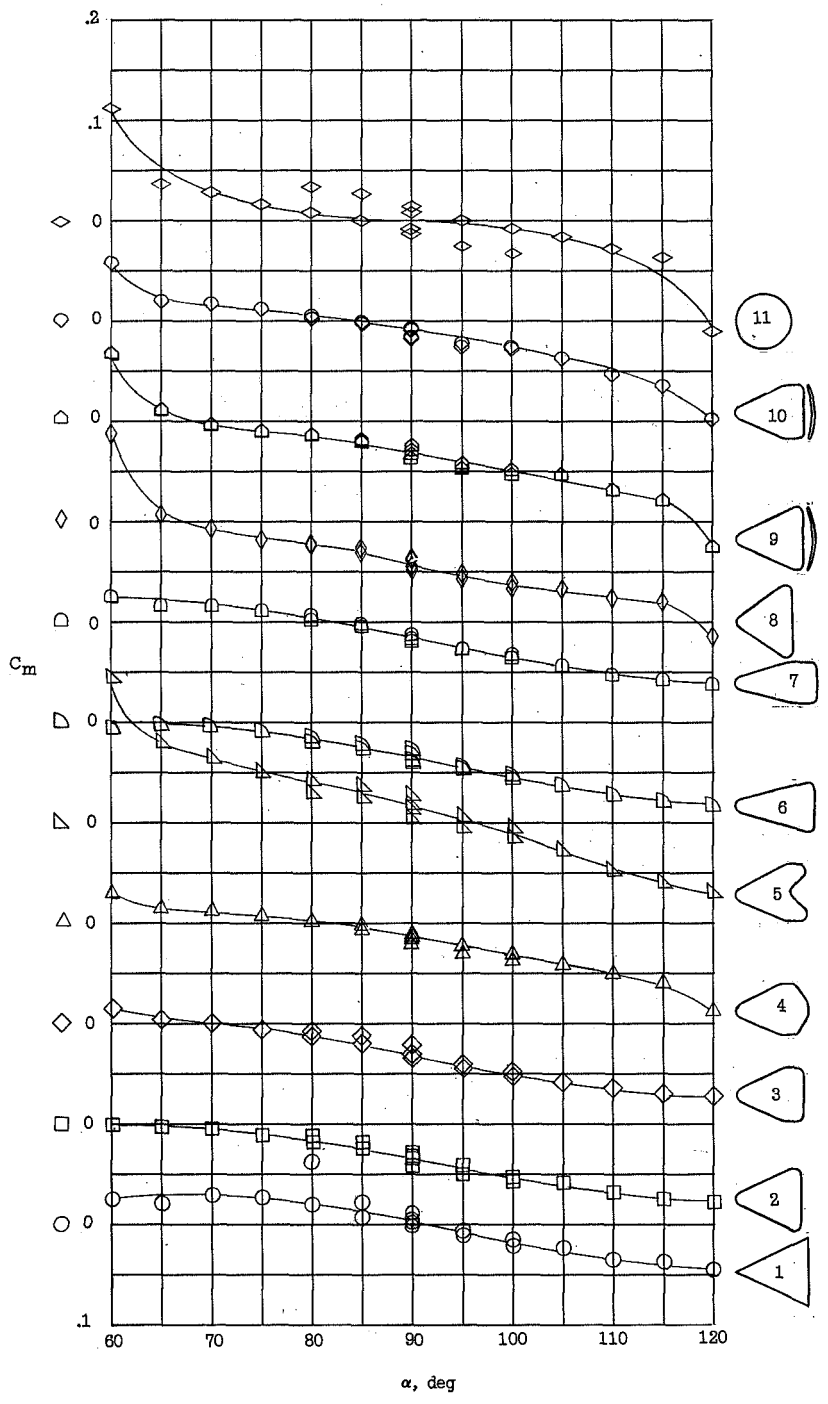

(c) Variation of pitching-moment coefficient with angle of attack.

Figure 5.- Continued.

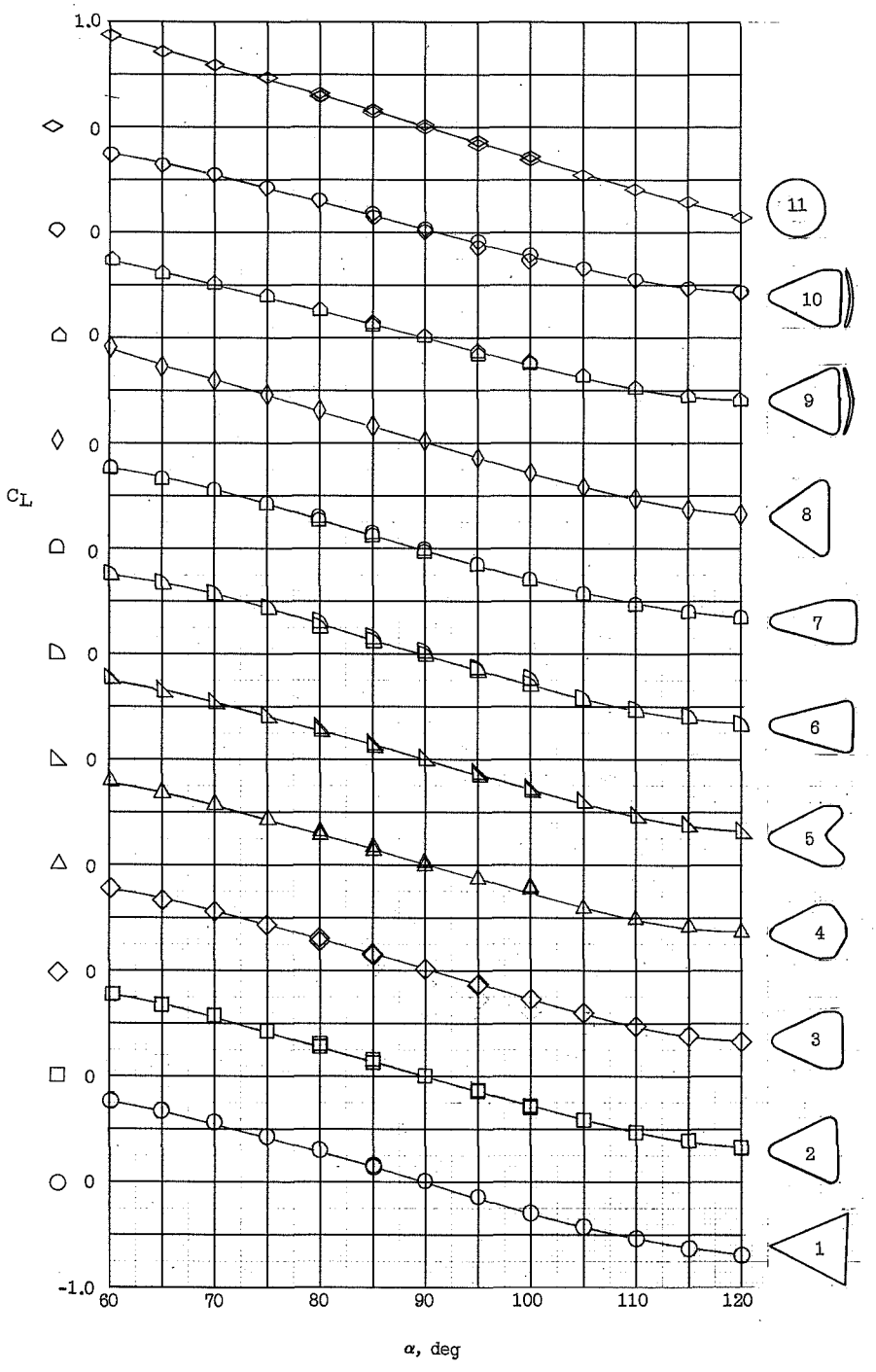

(d) Variation of lift coefficient with angle of attack.

Figure 5.- Continued.

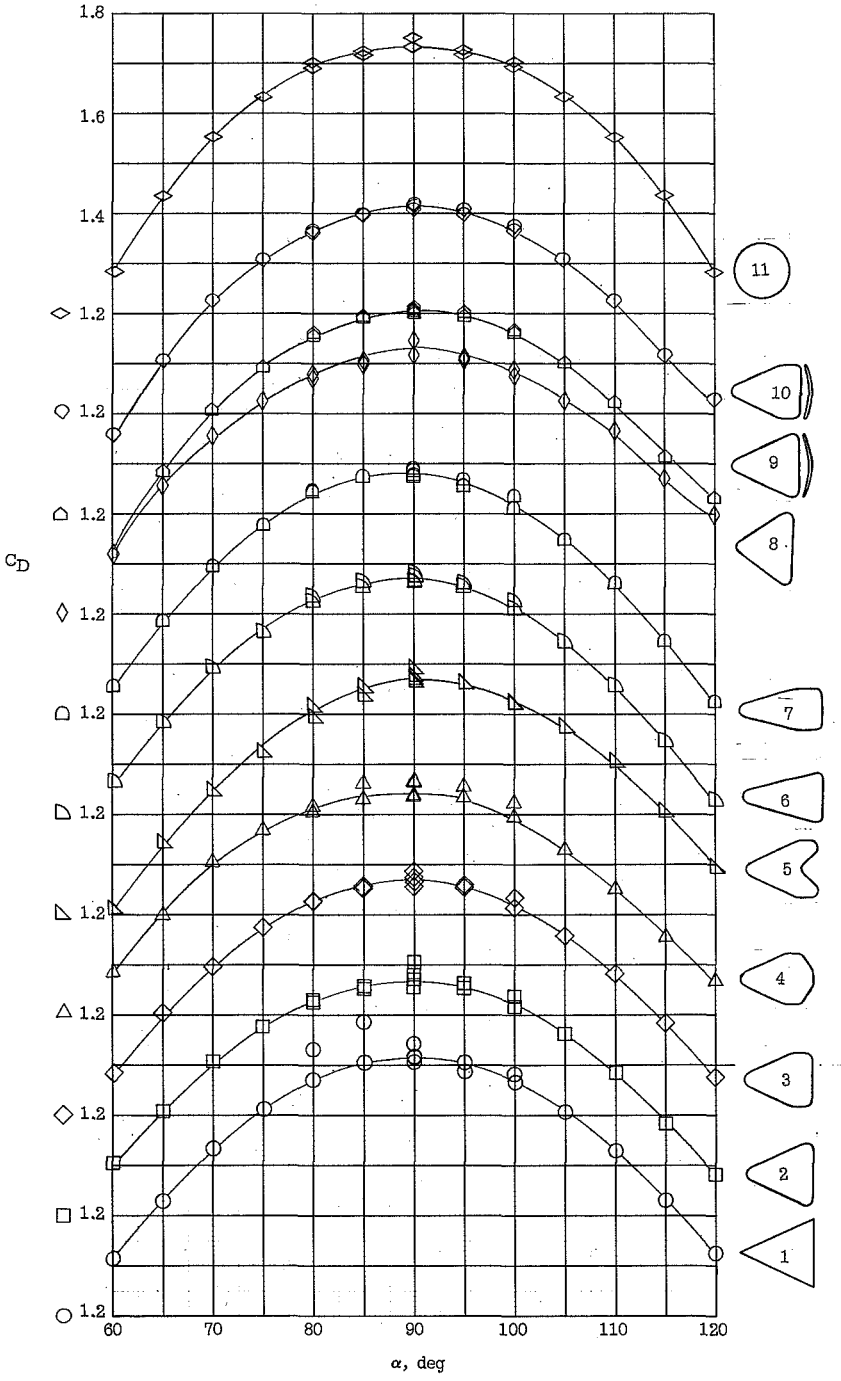

(e) Variation of drag coefficient with angle of attack.

Figure 5.- Continued.

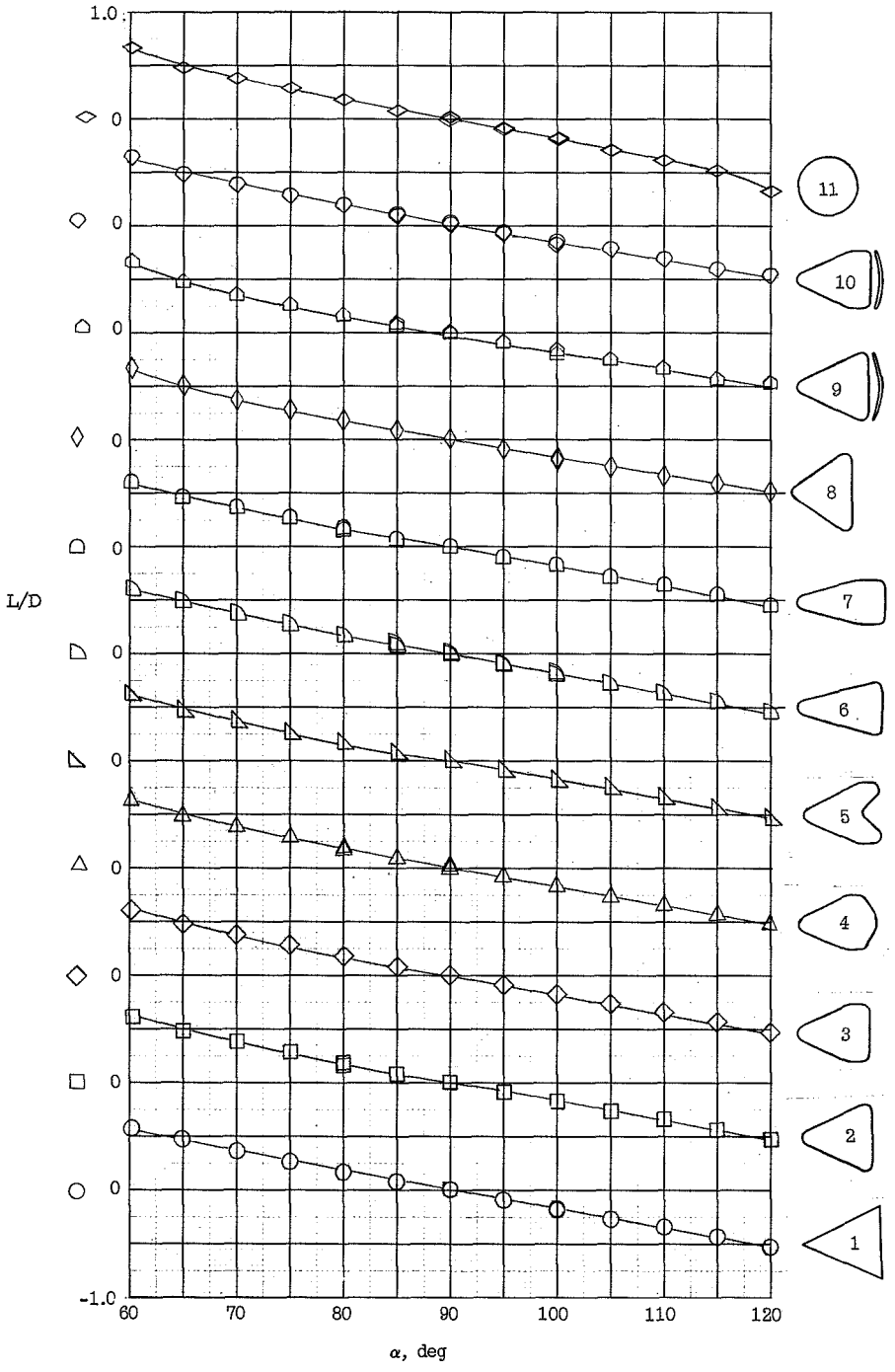

(f) Variation of lift-drag ratio with angle of attack.

Figure 5.- Continued.

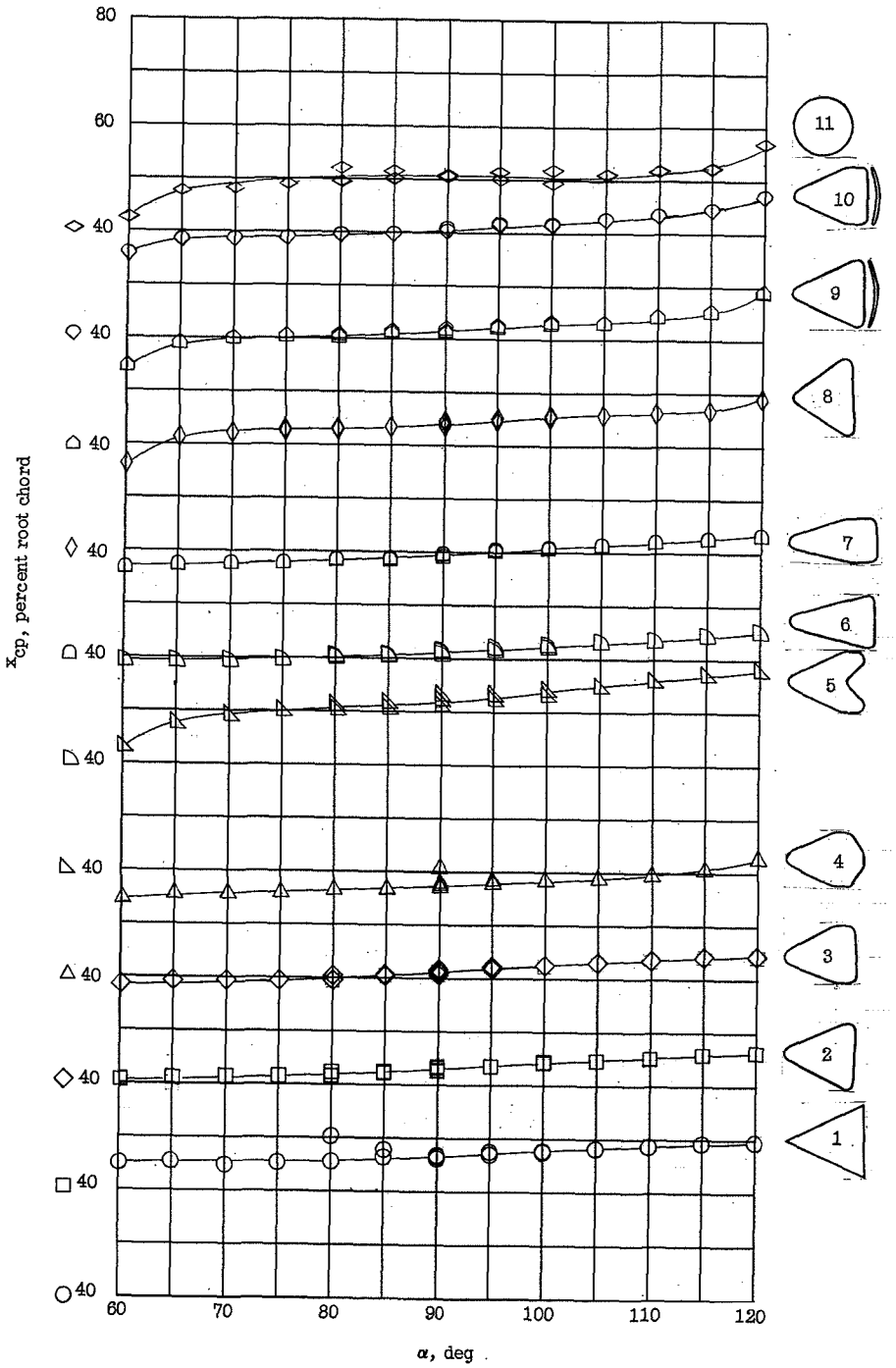

(g) Variation of longitudinal center of pressure with angle of attack.

Figure 5.- Continued.

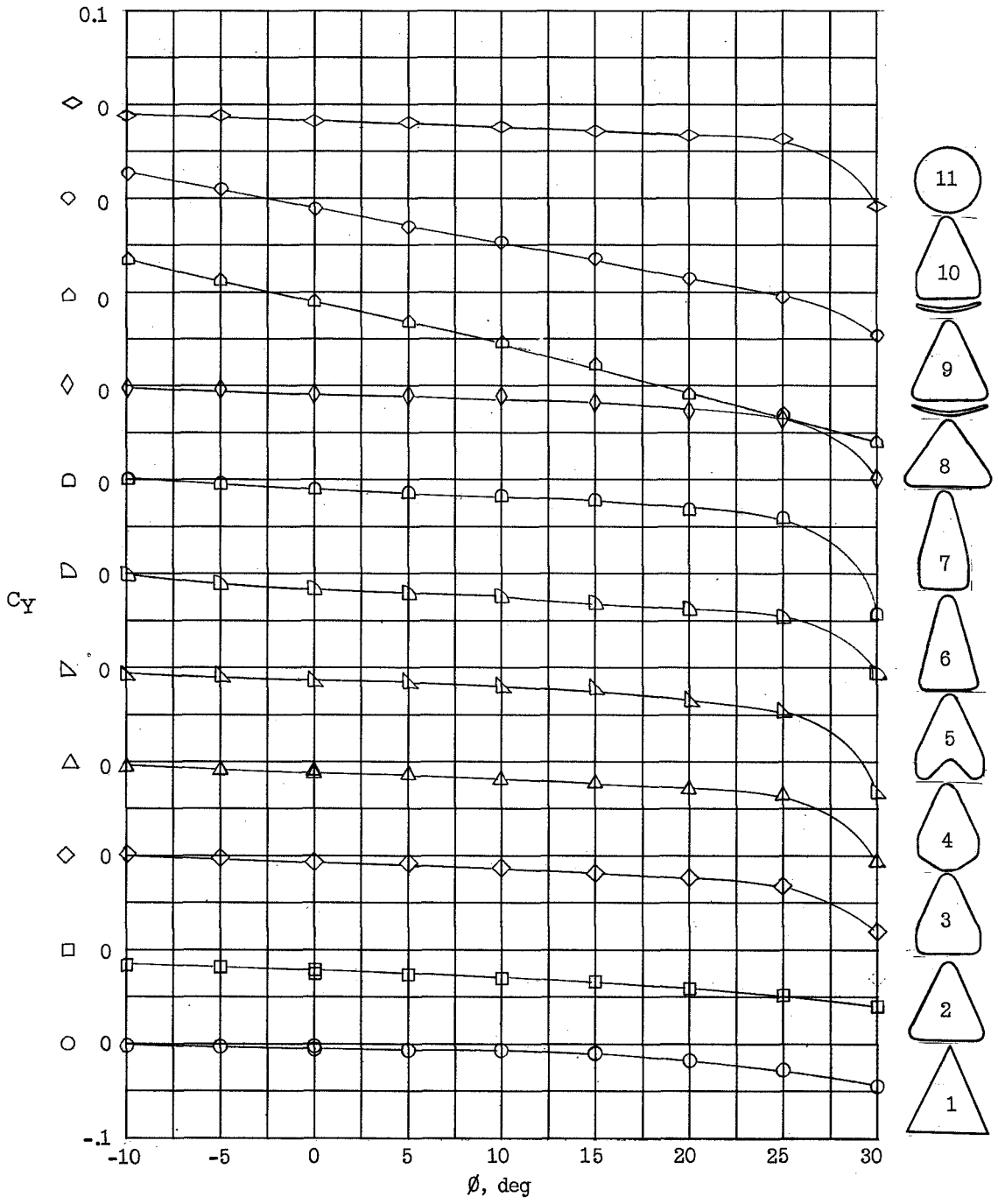

(h) Variation of side-force coefficient with roll angle at 90° angle of attack.

Figure 5.- Continued.

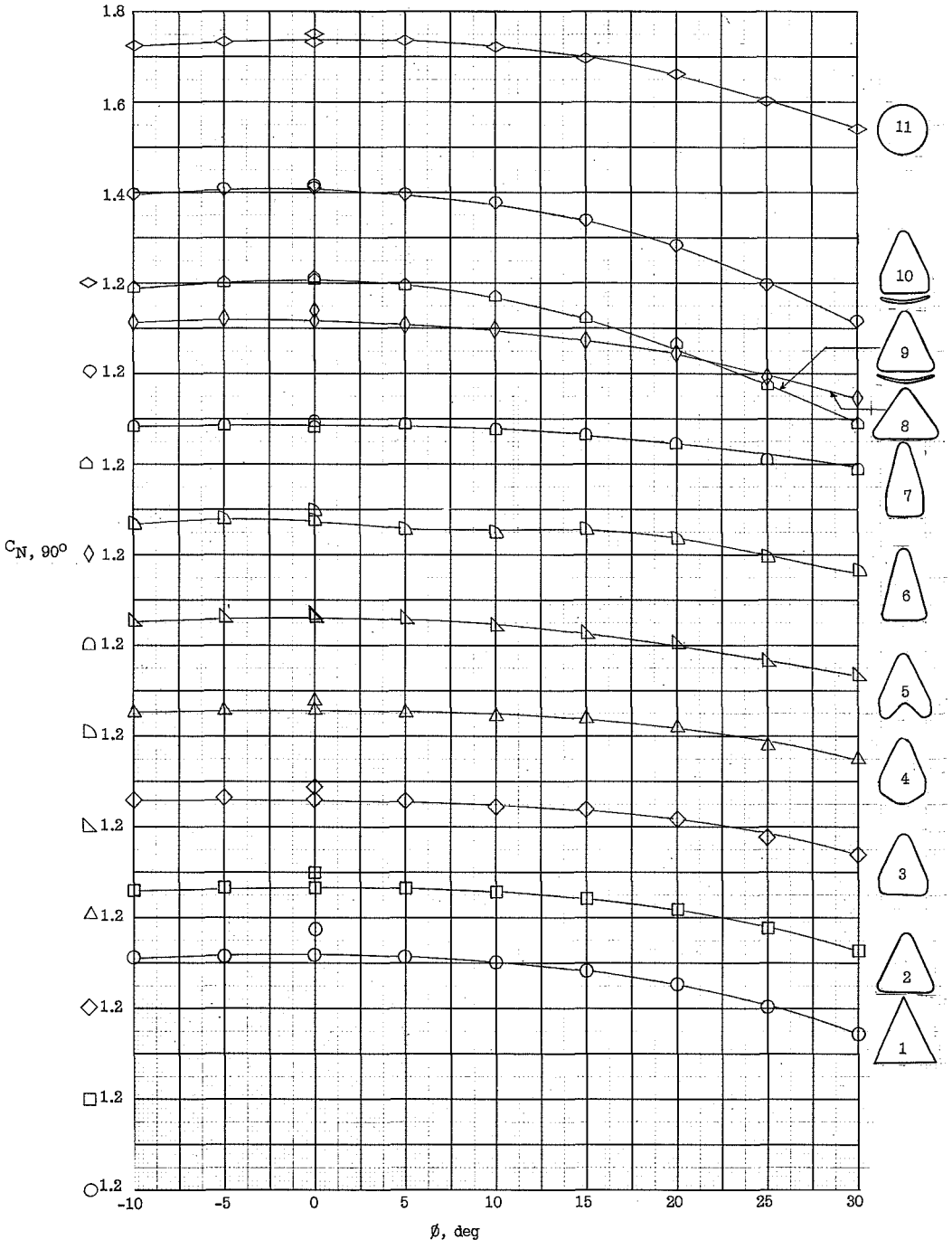

(i) Variation of normal-force coefficient with roll angle at 90° angle of attack.

Figure 5.- Continued.

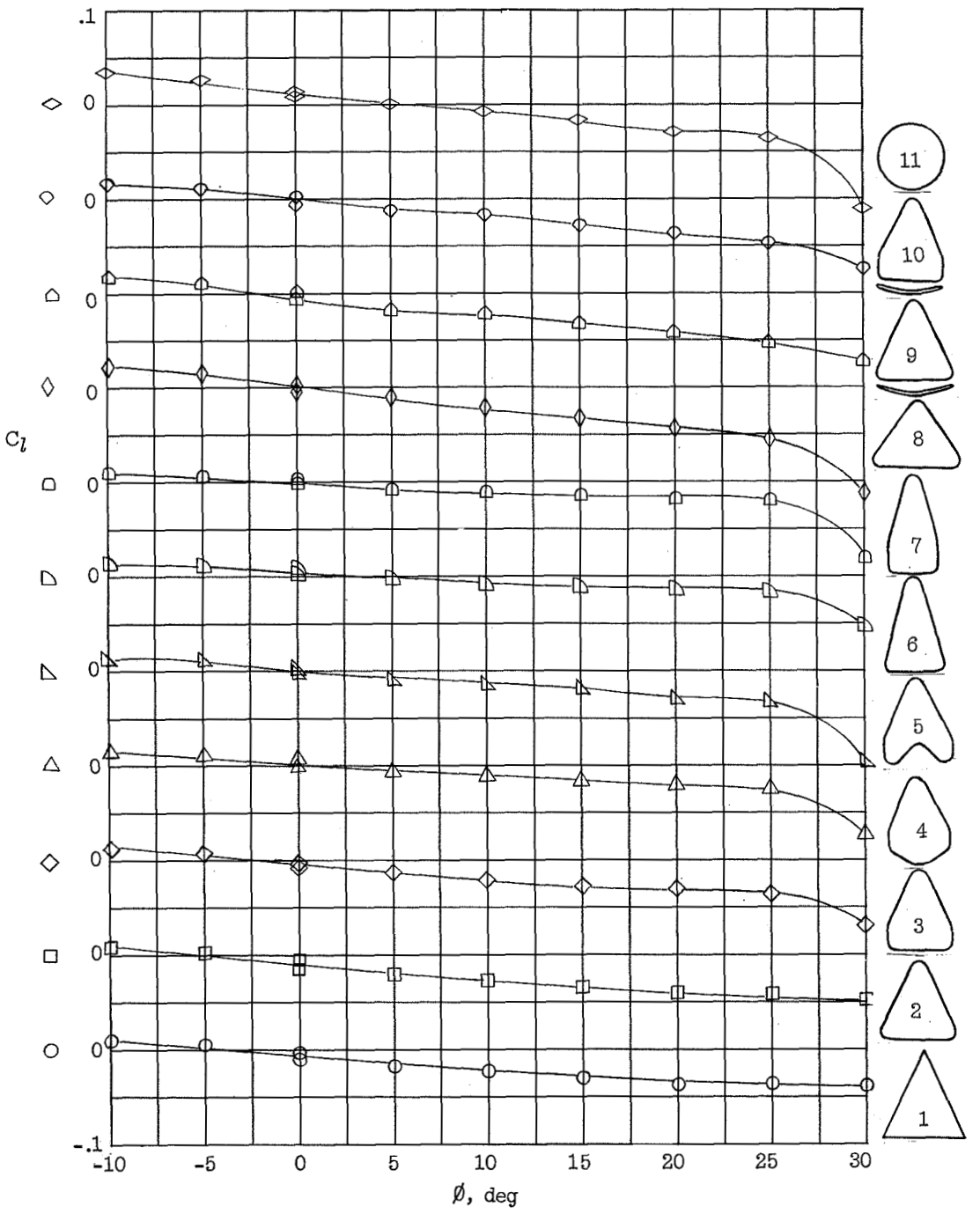

(j) Variation of rolling-moment coefficient with roll angle at 90° angle of attack.

Figure 5.- Continued.

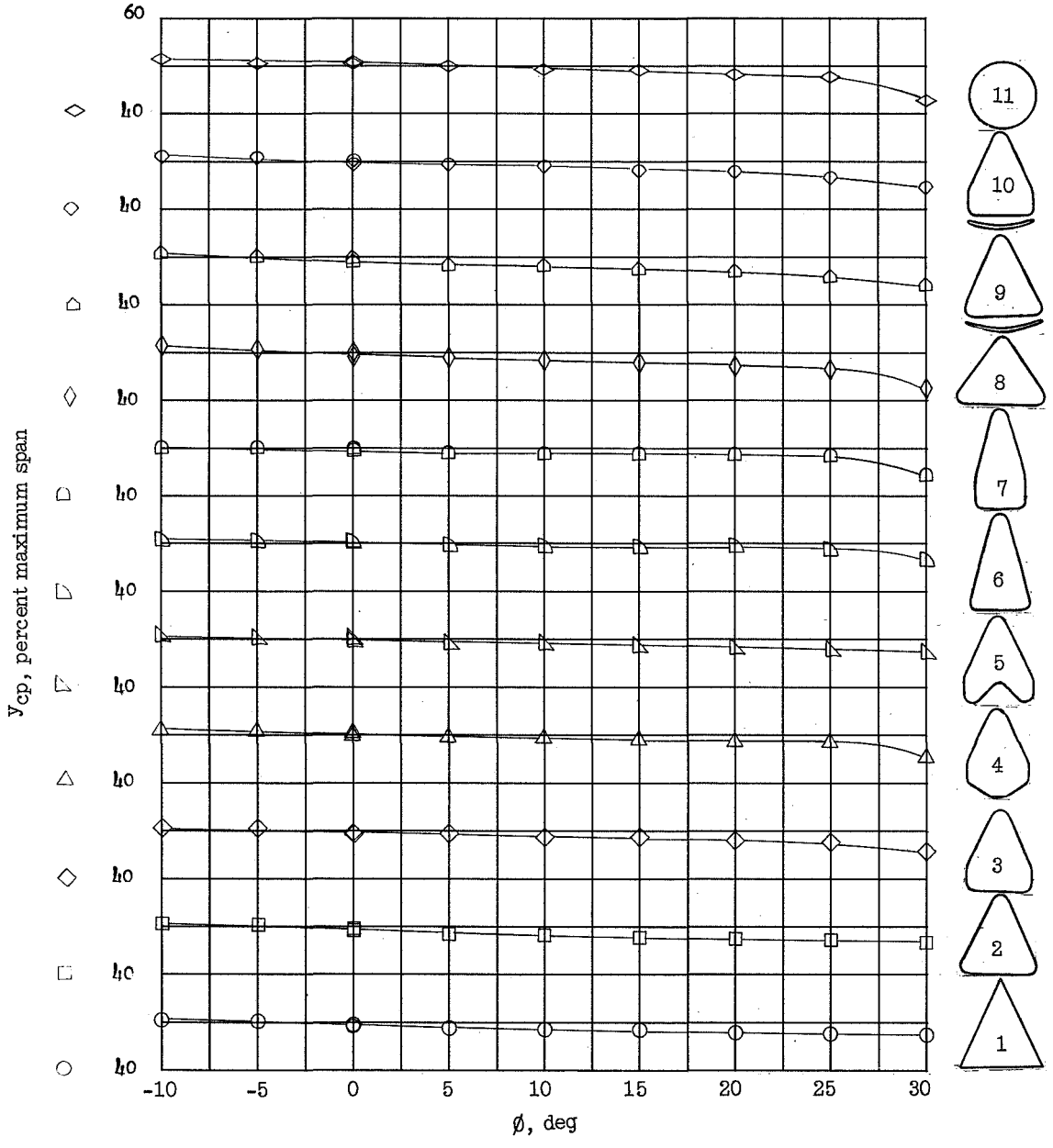

(k) Variation of lateral center of pressure with roll angle at 90° angle of attack.

Figure 5.- Concluded.

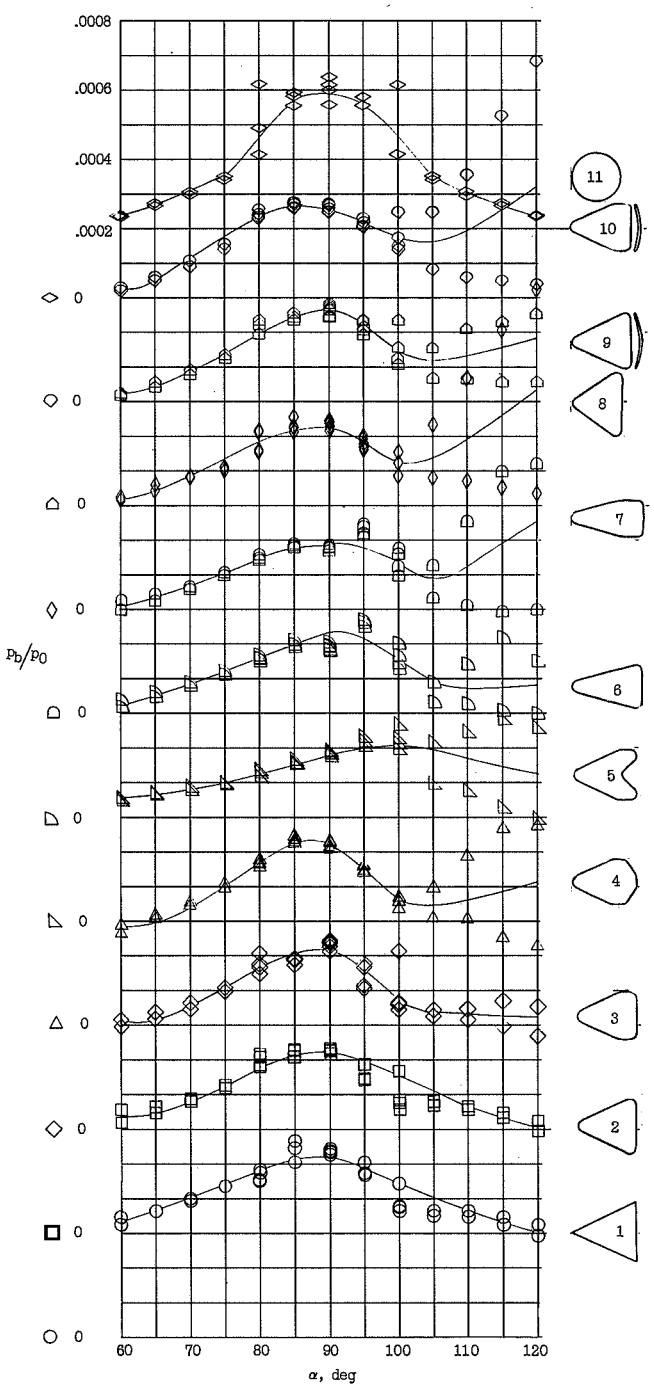

(a) Angle of attack.

Figure 6.- Variation of the ratio of base pressure to stagnation pressure with angle of attack and angle of roll.

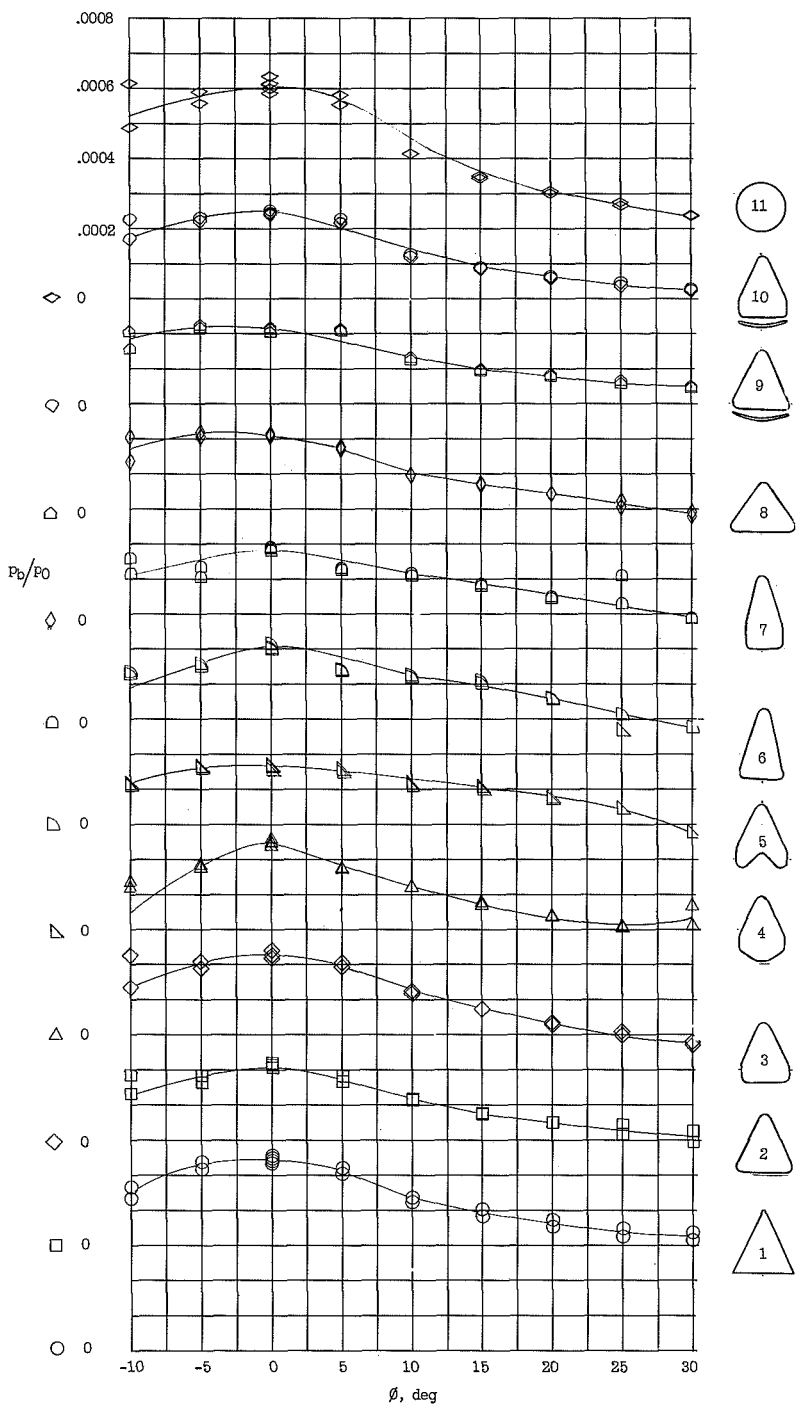

(b) Angle of roll.

Figure 6.- Concluded.

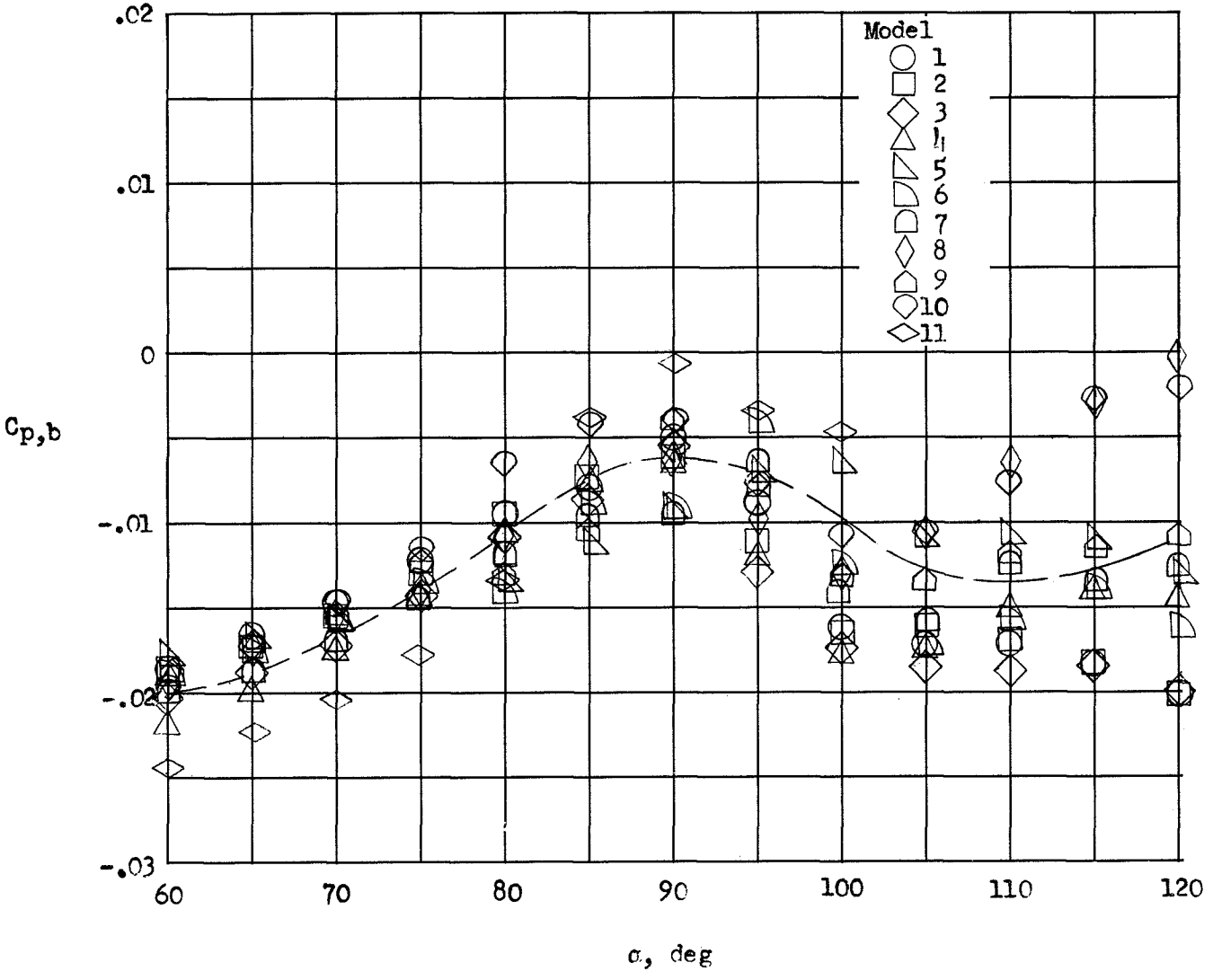

Figure 7.- Variation of base-pressure coefficient with angle of attack.

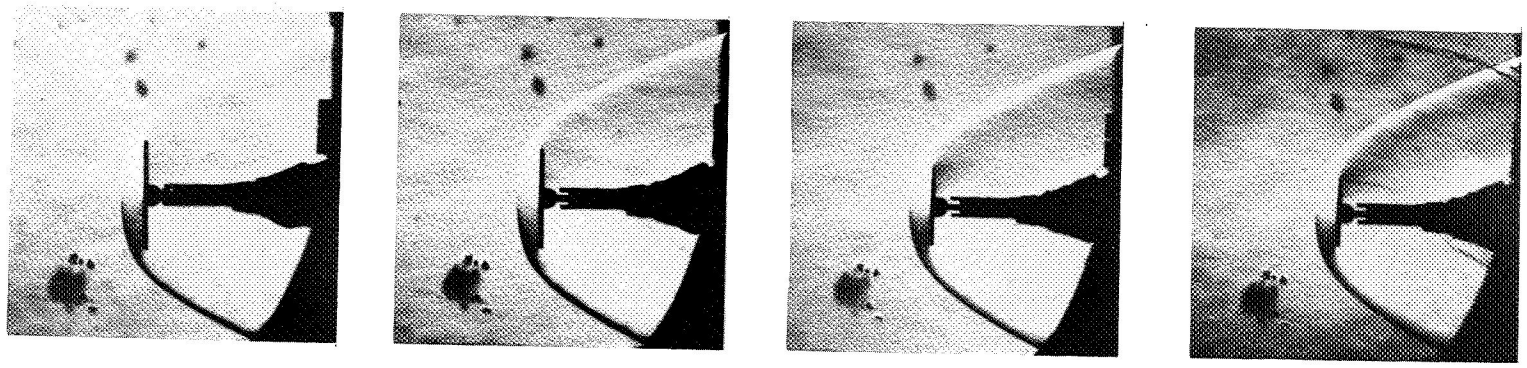

α, angle-of-attack position

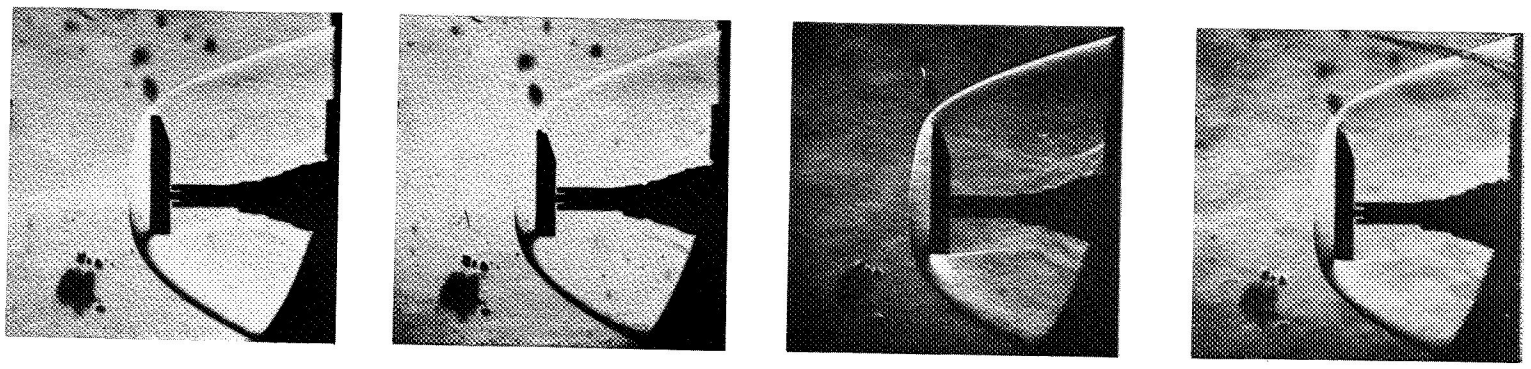

Model 1 Model 2 Model 6 Model 7

∅, angle-of-roll position

L-61-56

Figure 8.- Typical schlieren photographs of models at 90° angle of attack in the angle-of-roll position and angle-of-attack position.

α, angle-of-attack position

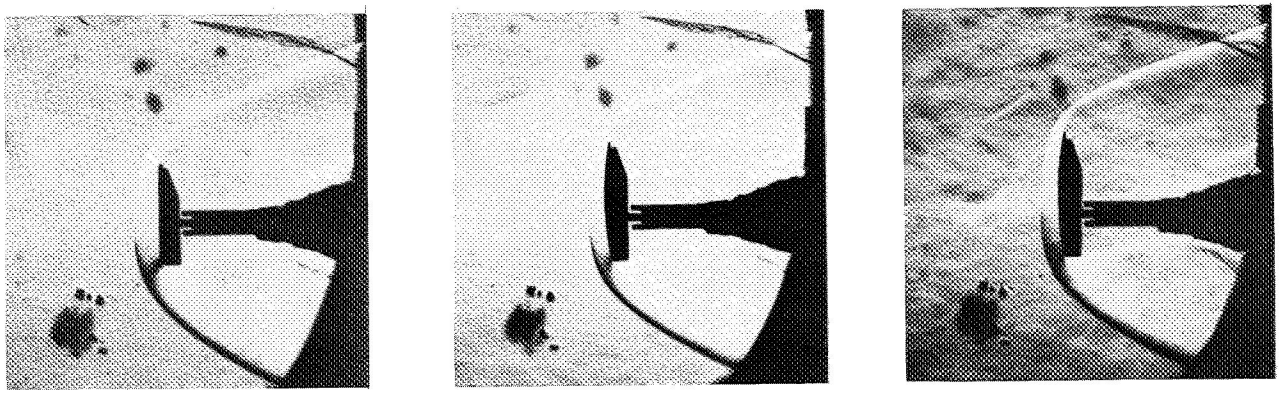

Model 8 Model 9 Model 10

ϕ, angle-of-roll position

Figure 8.- Concluded. L-61-57

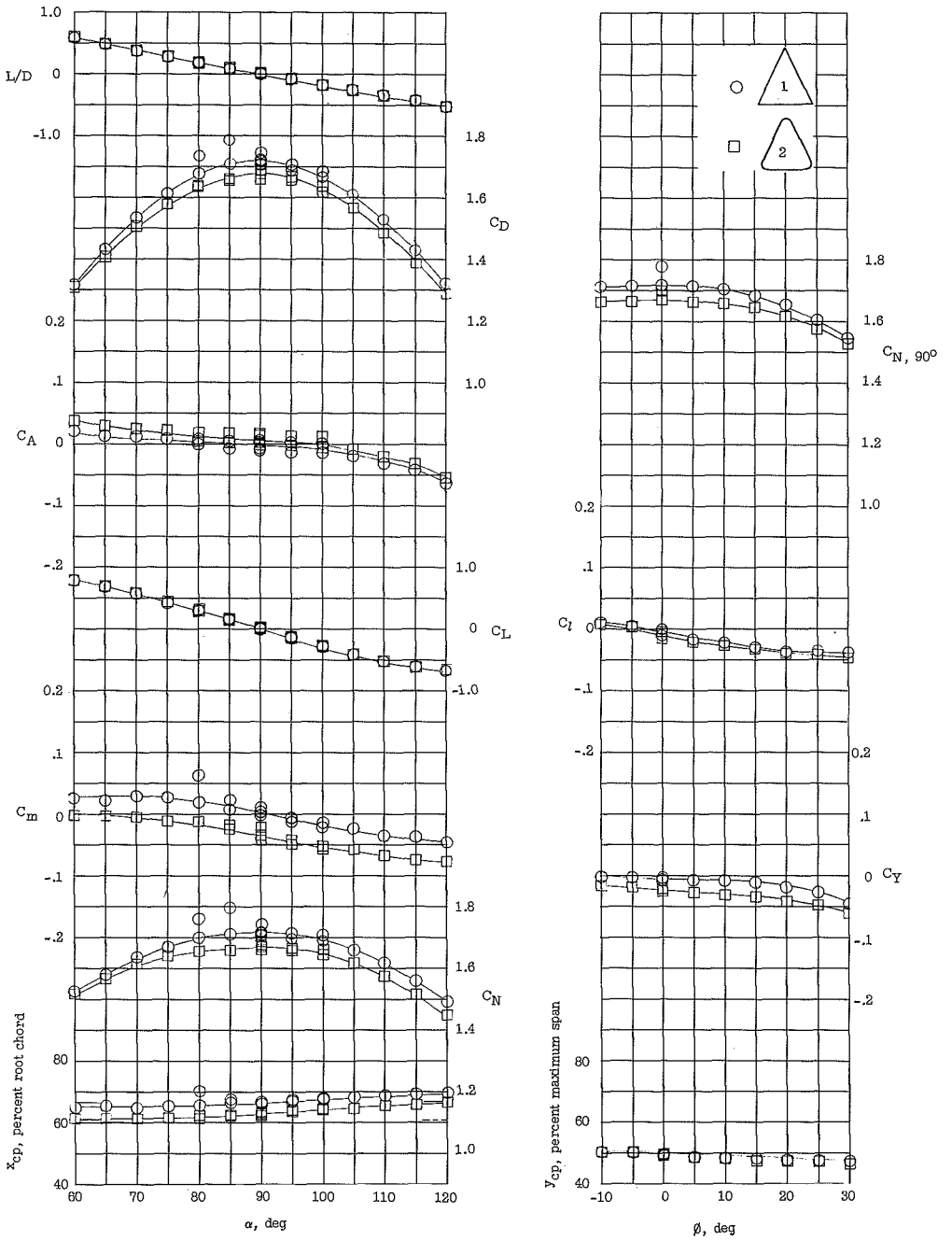

(a) Angle of attack.

(b) Angle of roll at 90° angle of attack.

Figure 9.- Effects of rounding corners and edges. (Solid and dashed lines indicate c.g. of models 1 and 2, respectively.)

L-12444

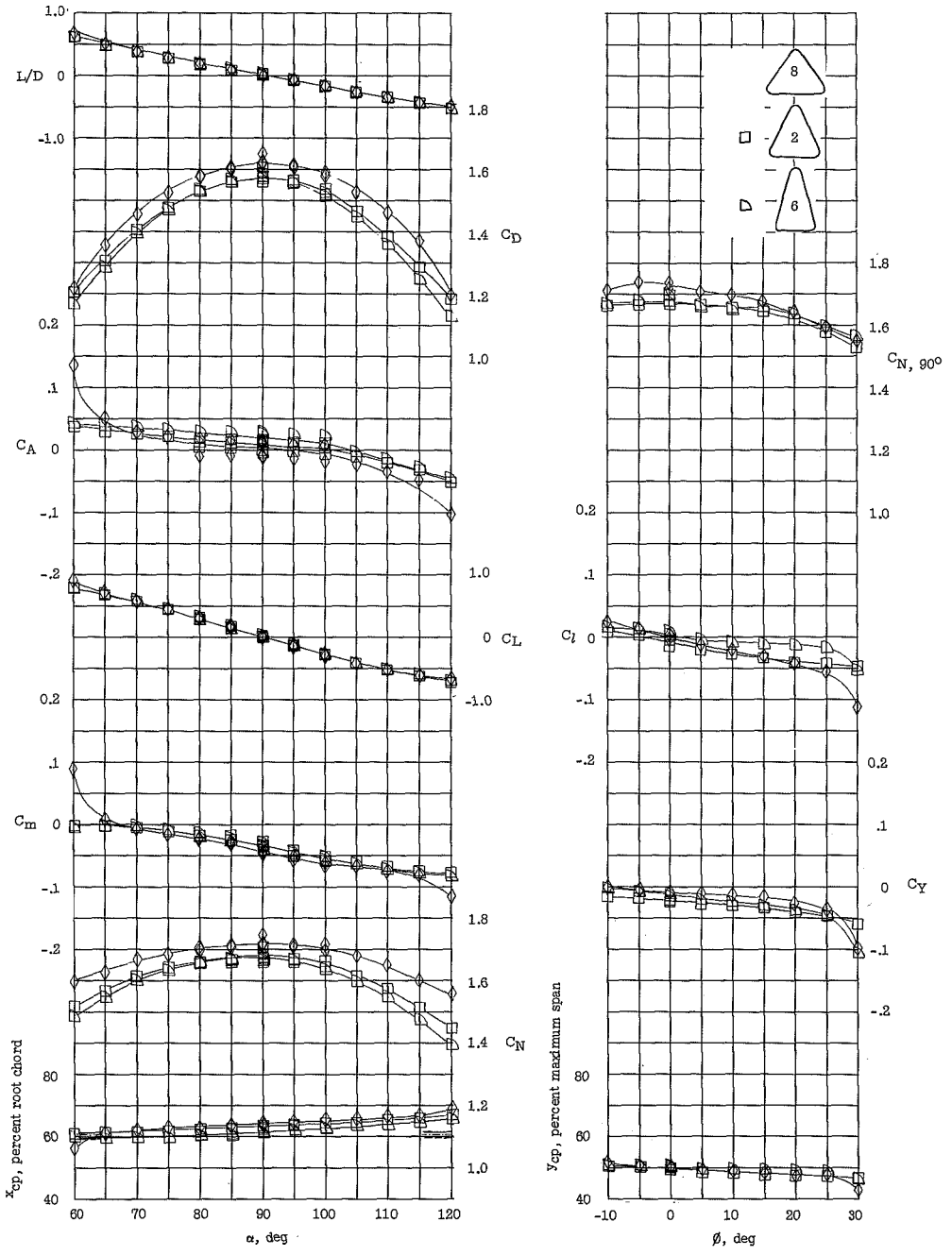

(a) Angle of attack.

(b) Angle of roll at 90° angle of attack.

Figure 10.- Effect of leading-edge sweep. (Solid, dash-dot, and dashed lines indicate c.g. of models 8, 2, and 6, respectively.)

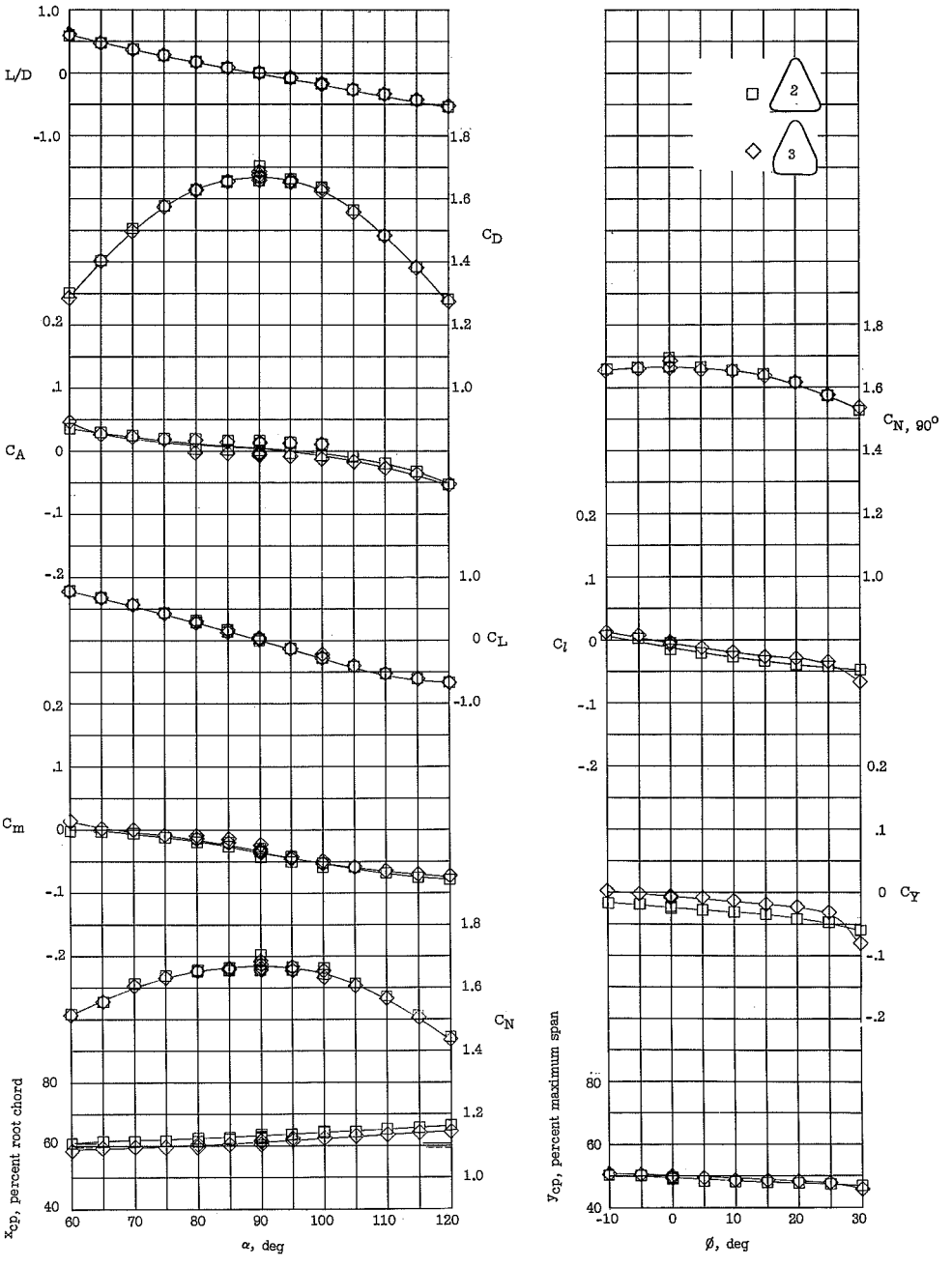

(a) 65° sweep, flat-bottom models at angles of attack.

(b) 65° sweep, flat-bottom models at angle of roll at 90° angle of attack.

Figure 11.- Effects of clipping wing tips. (Solid and dashed lines indicate c.g. of unclipped and clipped models, respectively.)

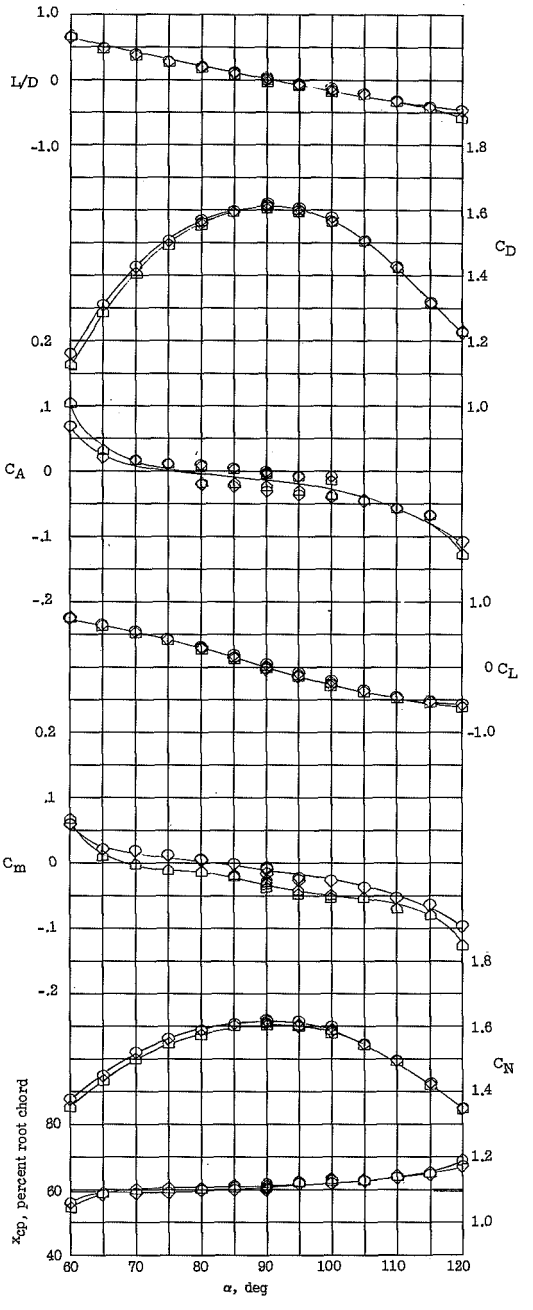

(c) 65° sweep, rounded-bottom models at angles of attack.

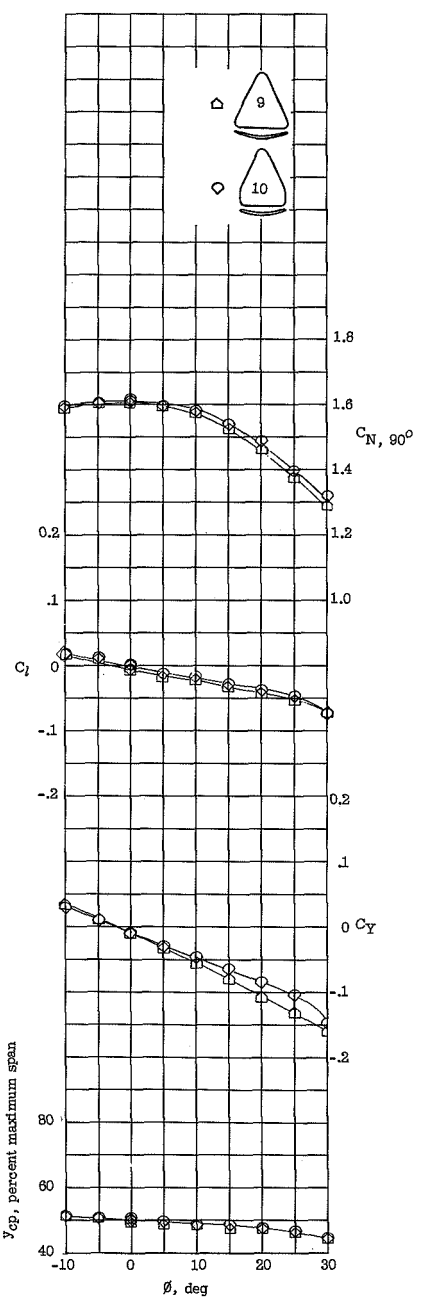

(d) 65° sweep, rounded-bottom models at angle of roll at 90° angle of attack.

Figure 11.- Continued.

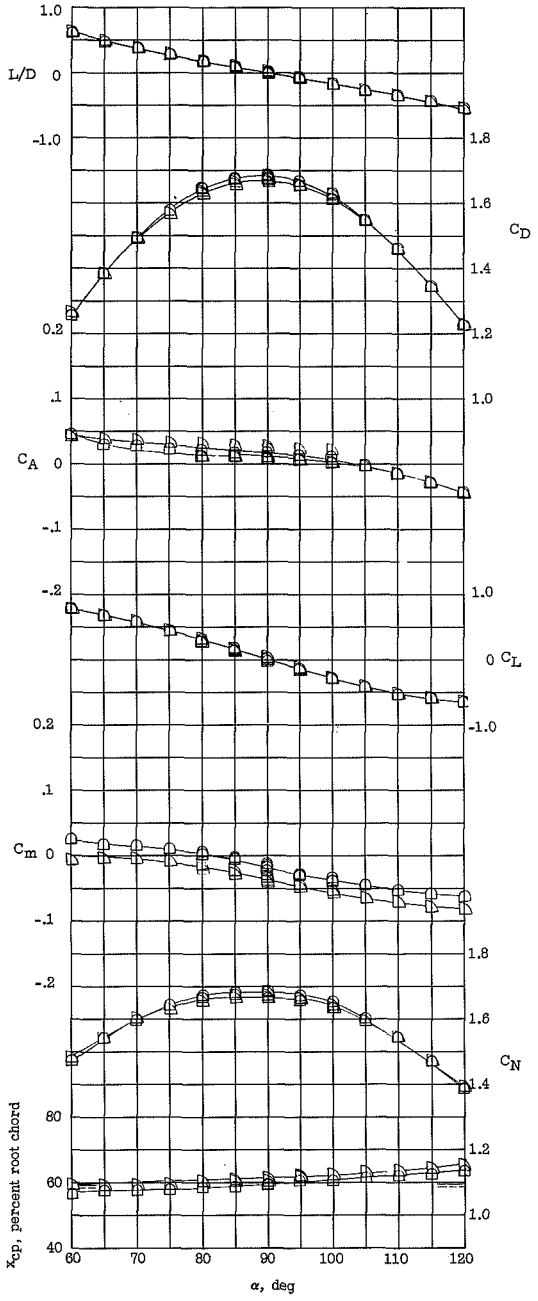

(e) 75° sweep, flat-bottom models at angles of attack.

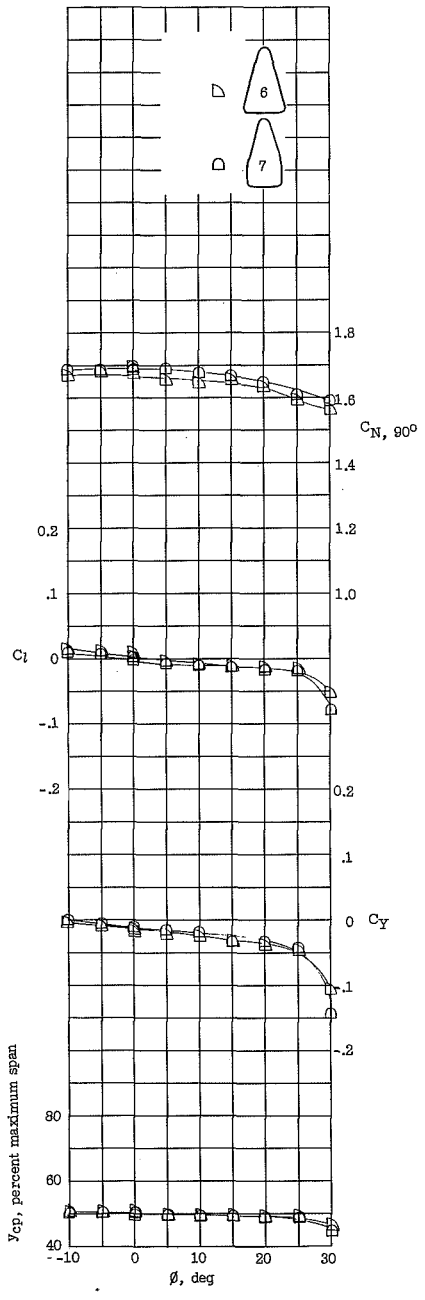

(f) 75° sweep, flat-bottom models at angle of roll at 90° angle of attack.

Figure 11.- Concluded.

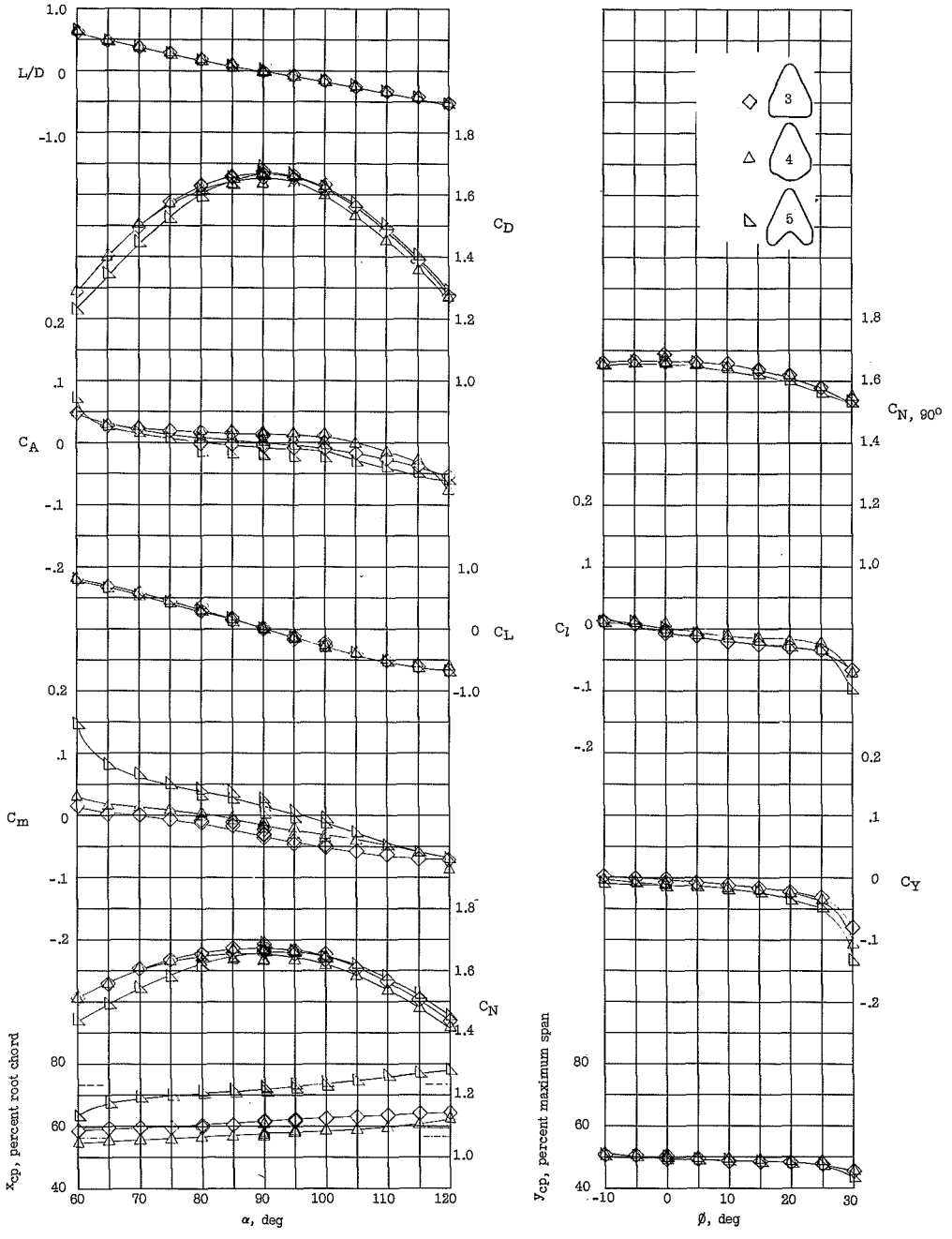

(a) Angle of attack.

(b) Angle of roll at 90° angle of attack.

Figure 12.- Effects of trailing-edge sweep. (Solid, dash-dot, and dashed lines indicate c.g. of models 3, 4, and 5, respectively.)

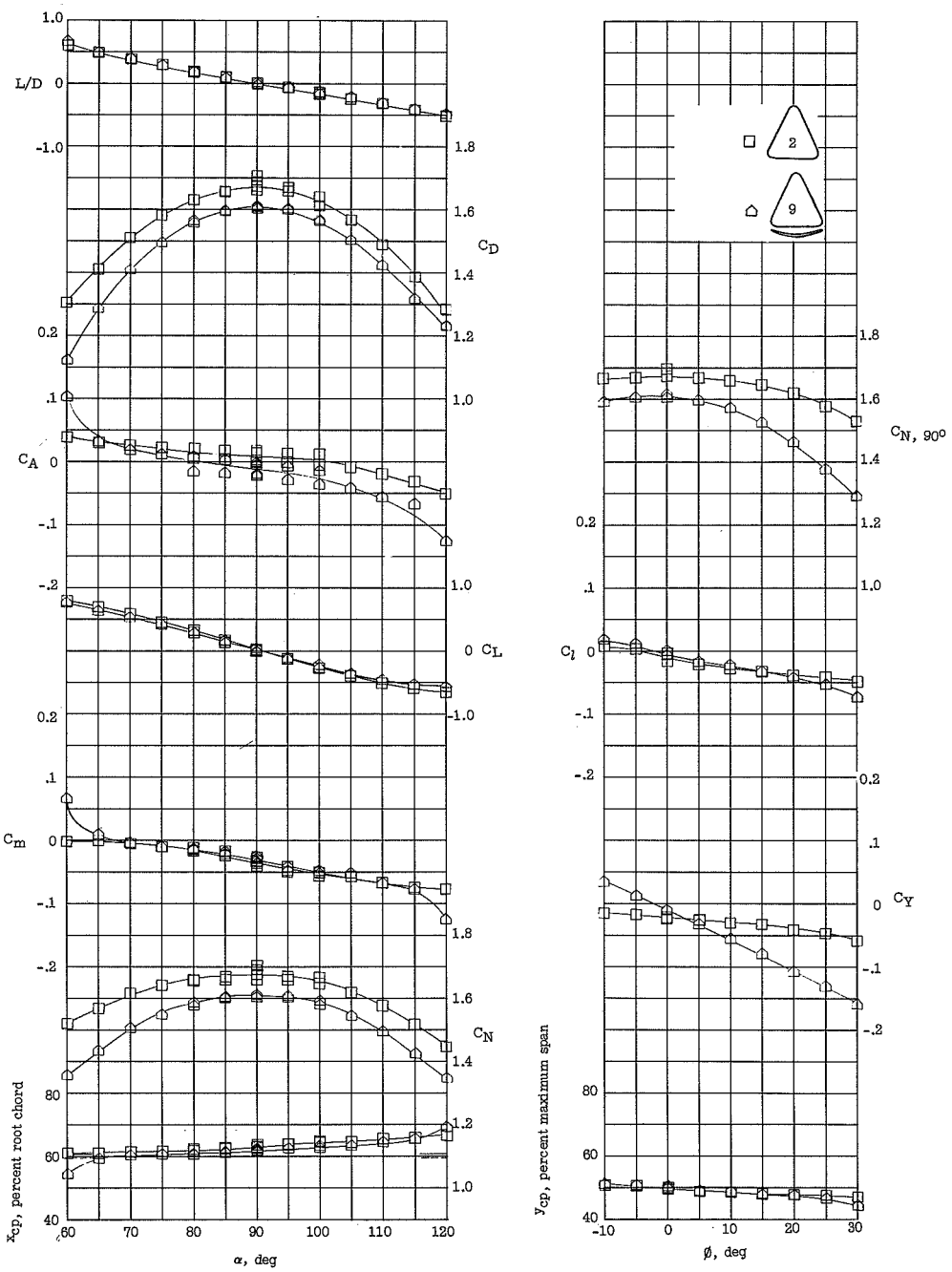

(a) 65° sweep models at angles of attack.

(b) 65° sweep models at angles of roll at 90° angle of attack.

Figure 13.- Effects of rounding bottoms. (Solid and dashed lines indicate c.g. of flat- and rounded-bottom models, respectively.)

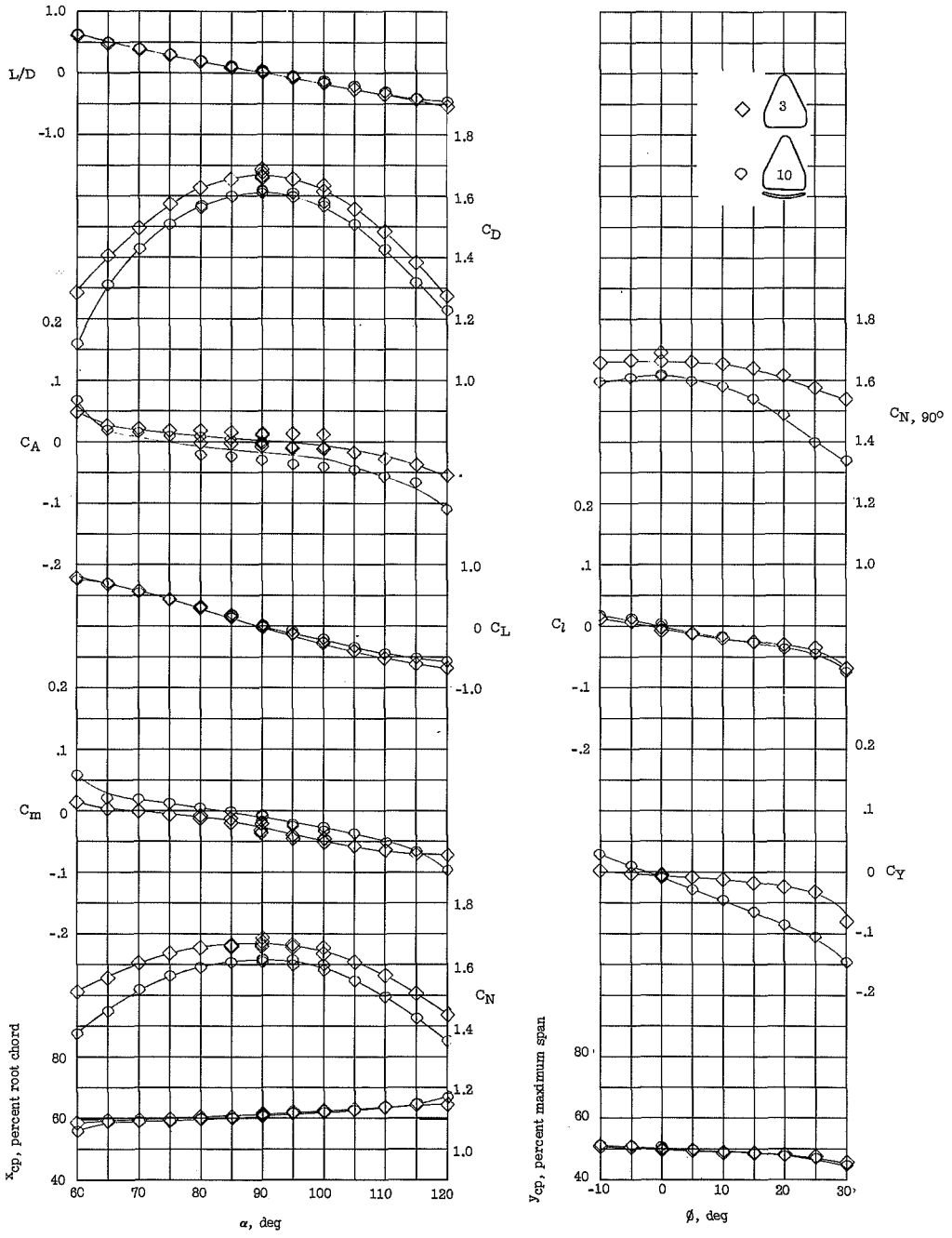

(c) 65° sweep models with clipped tips at angles of attack.

(d) 65° sweep models with clipped tips at angle of roll at 90° angle of attack.

Figure 13.- Concluded.

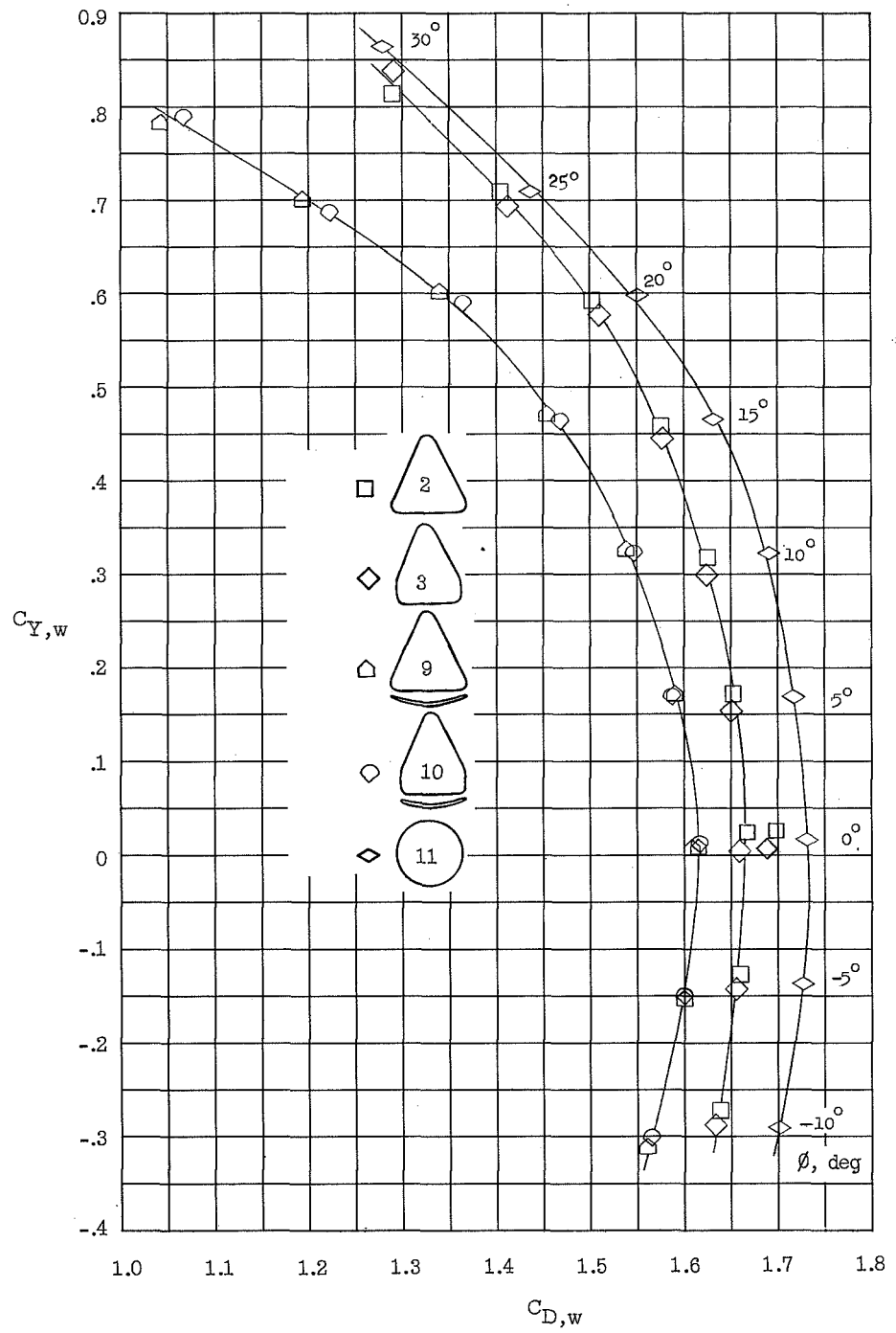

Figure 14.- Variation of $C_{D,w}$ with $C_{Y,w}$ on the wind axes at 90° angle of attack for various roll angles showing the effect on lateral-range potential of geometric changes on winged-type reentry vehicles.

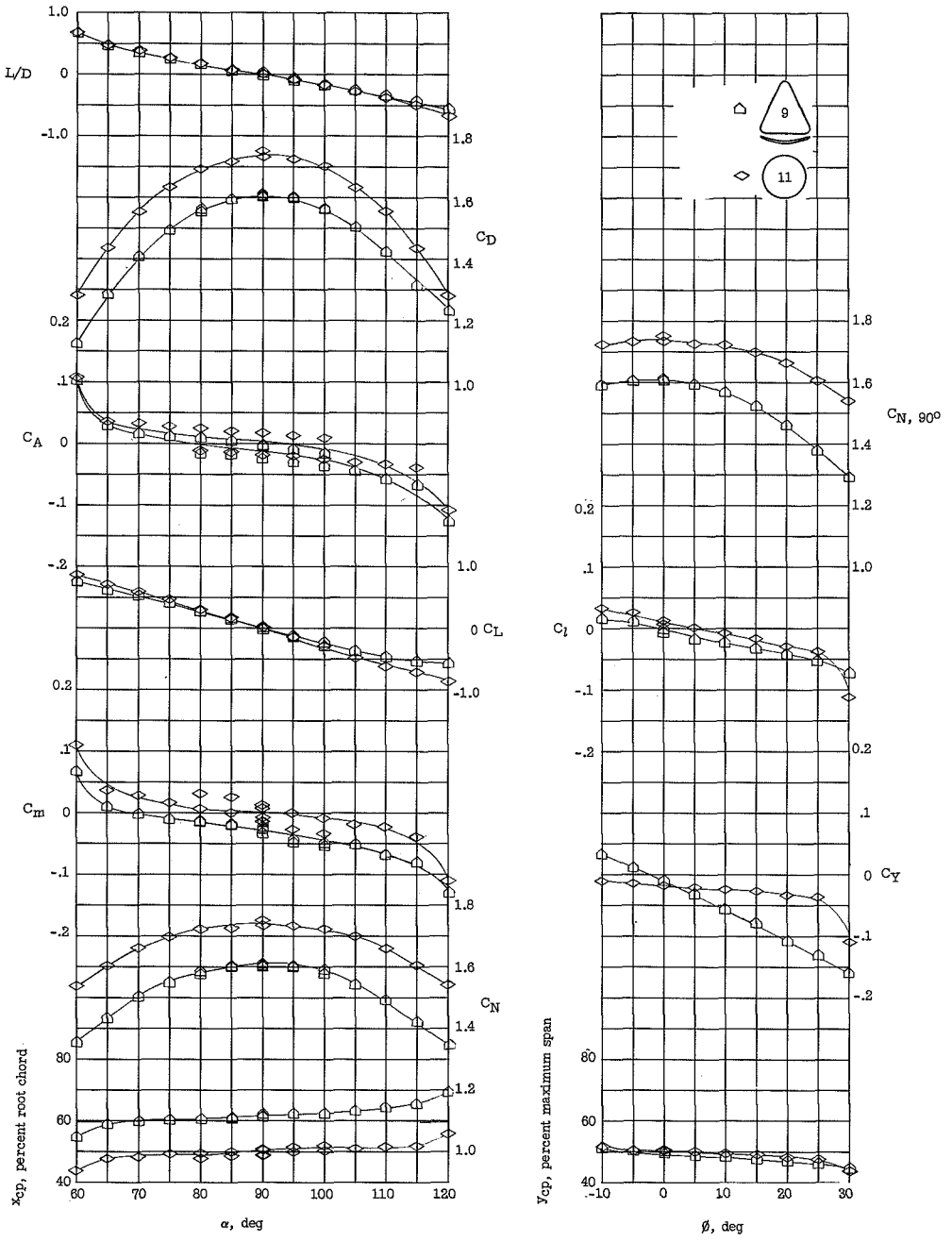

(a) Angle of attack.

(b) Angle of roll at 90° angle of attack.

Figure 15.- Comparison of rounded-bottom delta and circular planform wings. (Solid and dashed lines indicate c.g. of models 9 and 11, respectively.)

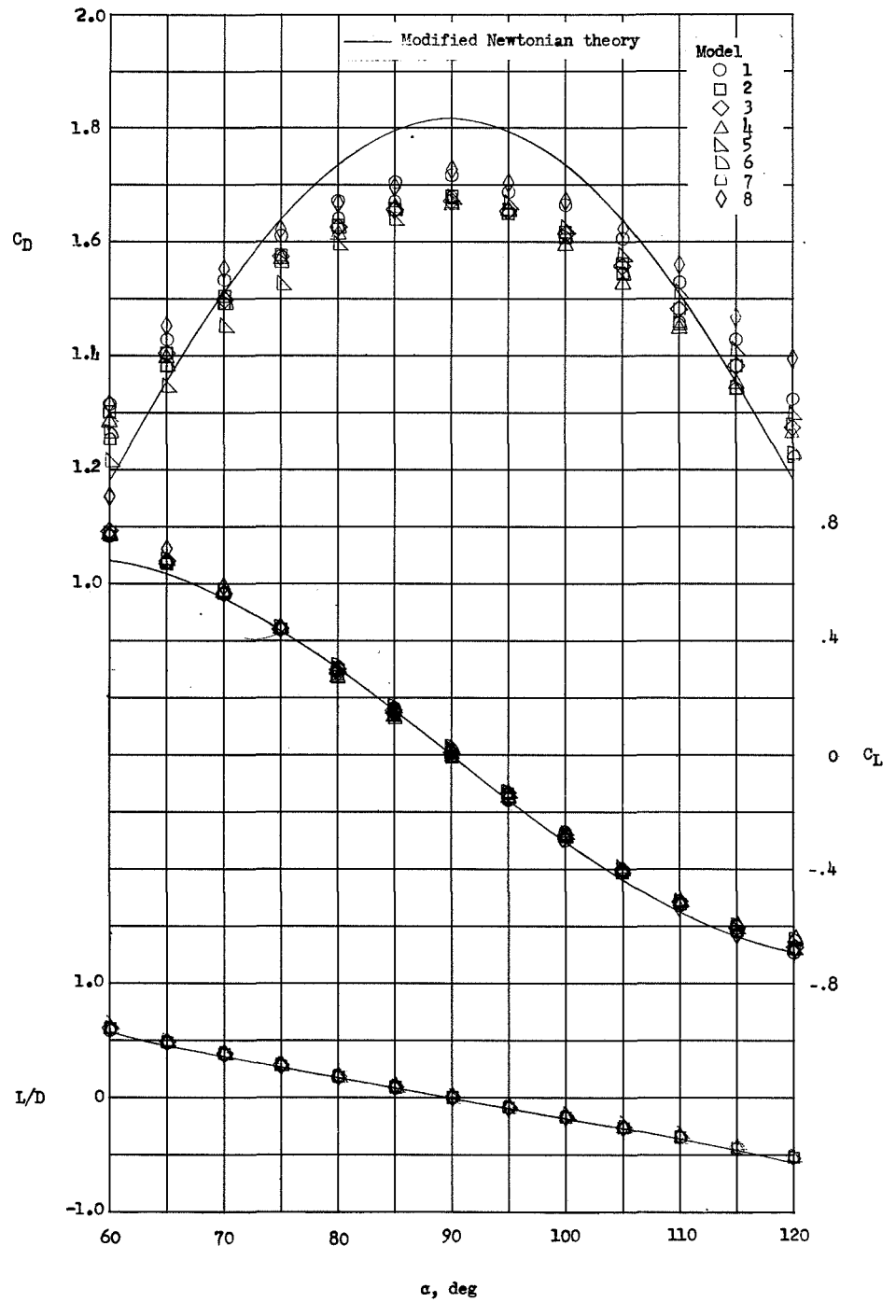

Figure 16.- A comparison of lift, drag, and lift-drag ratio for the flat-bottom models with the predicted values by modified Newtonian theory with $C_{p,max}$ of 1.818.

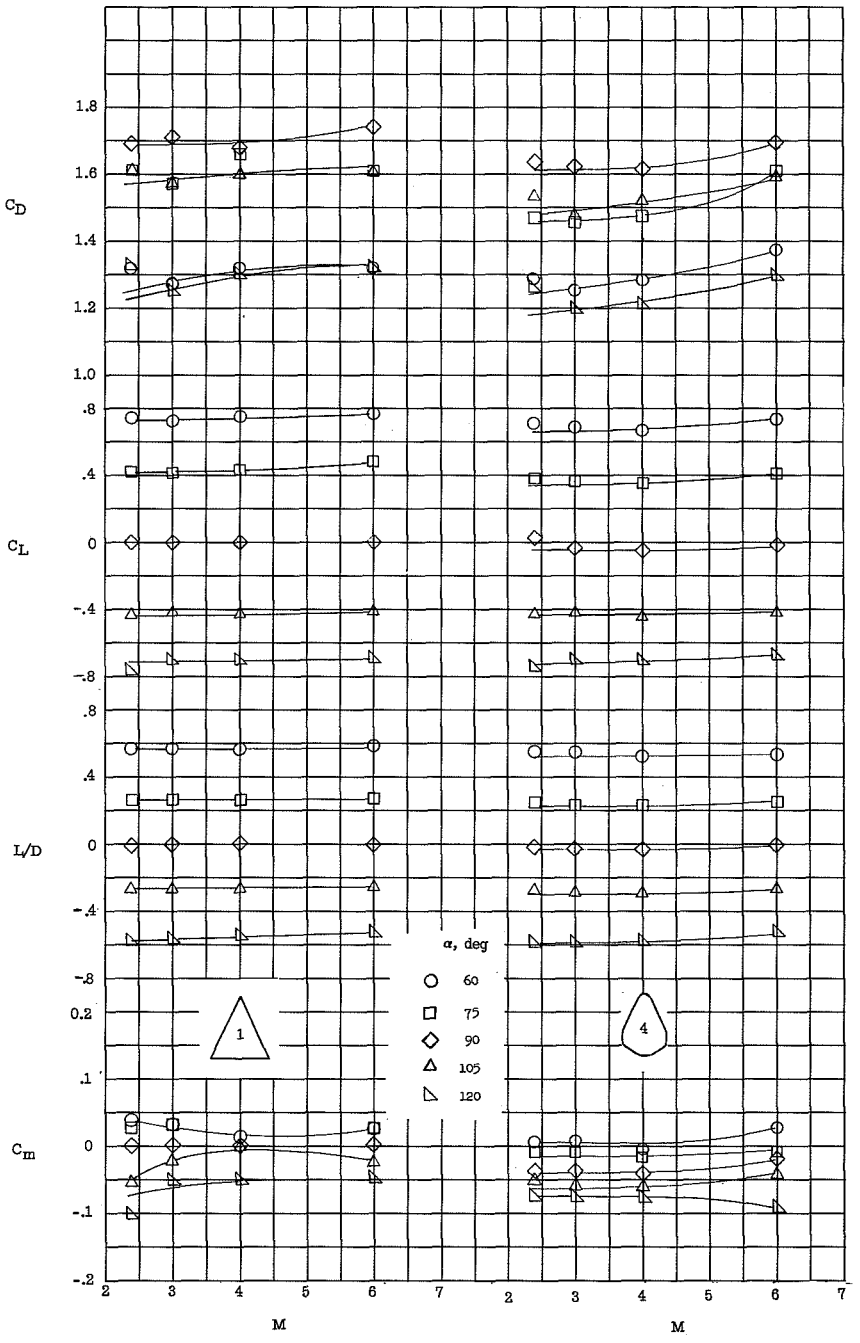

(a) Model 1. (b) Model 4.

Figure 17.- Variation of force and moment coefficients with Mach number for a group of winged reentry vehicles at various angles of attack and roll.

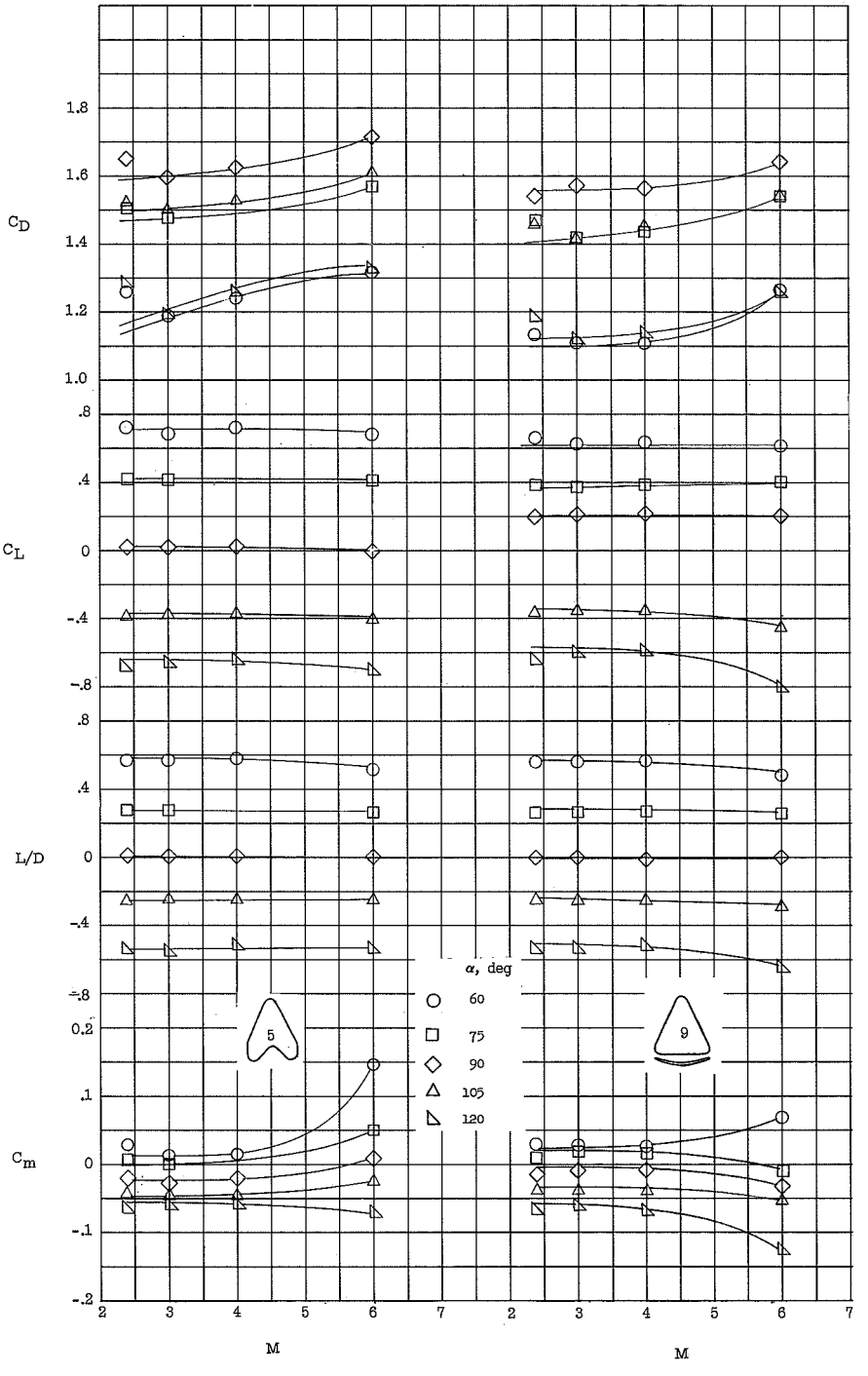

(c) Model 5.

(d) Model 9.

Figure 17.- Continued.

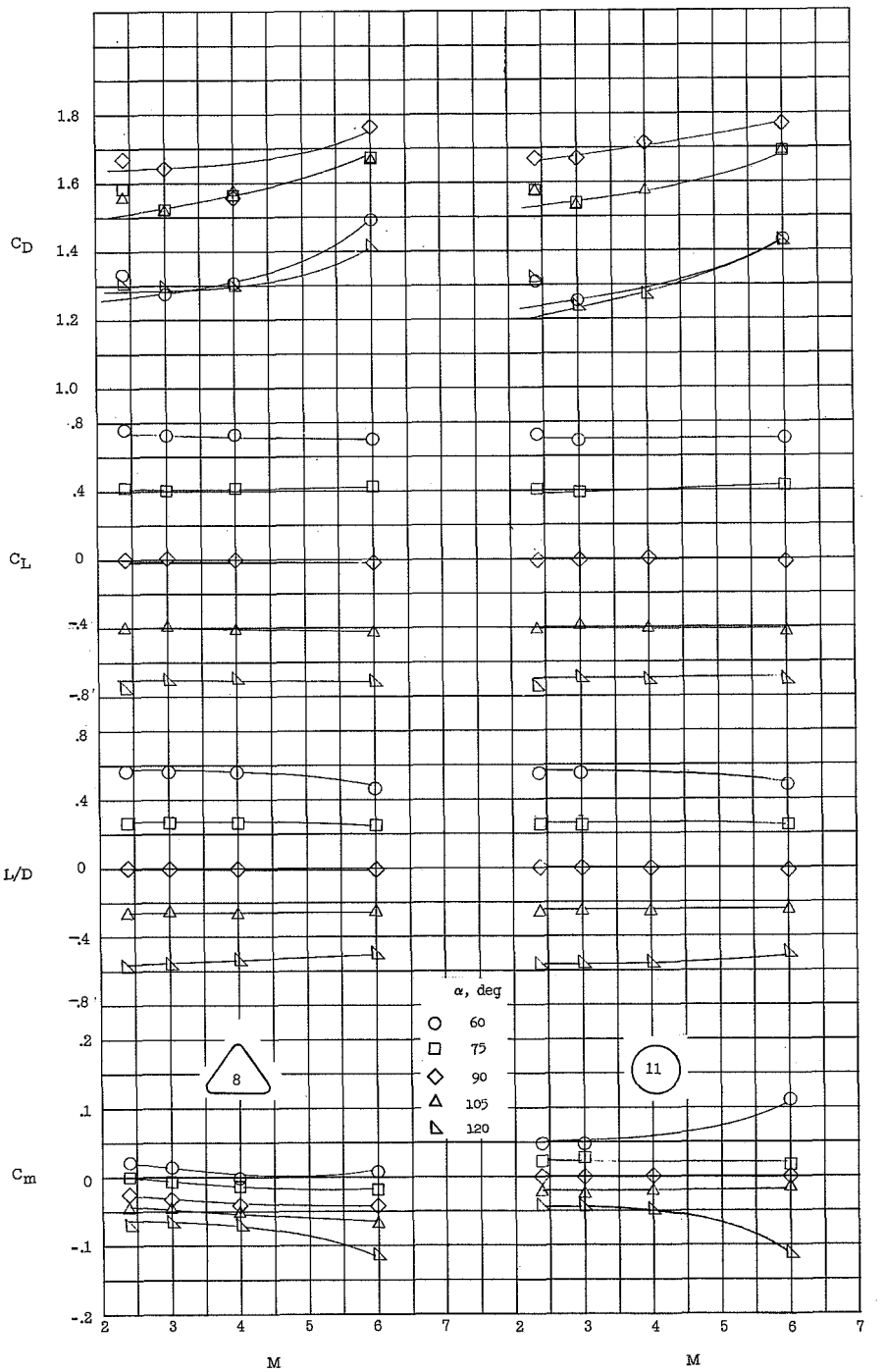

(e) Model 8.

(f) Model 11.

Figure 17.- Continued.

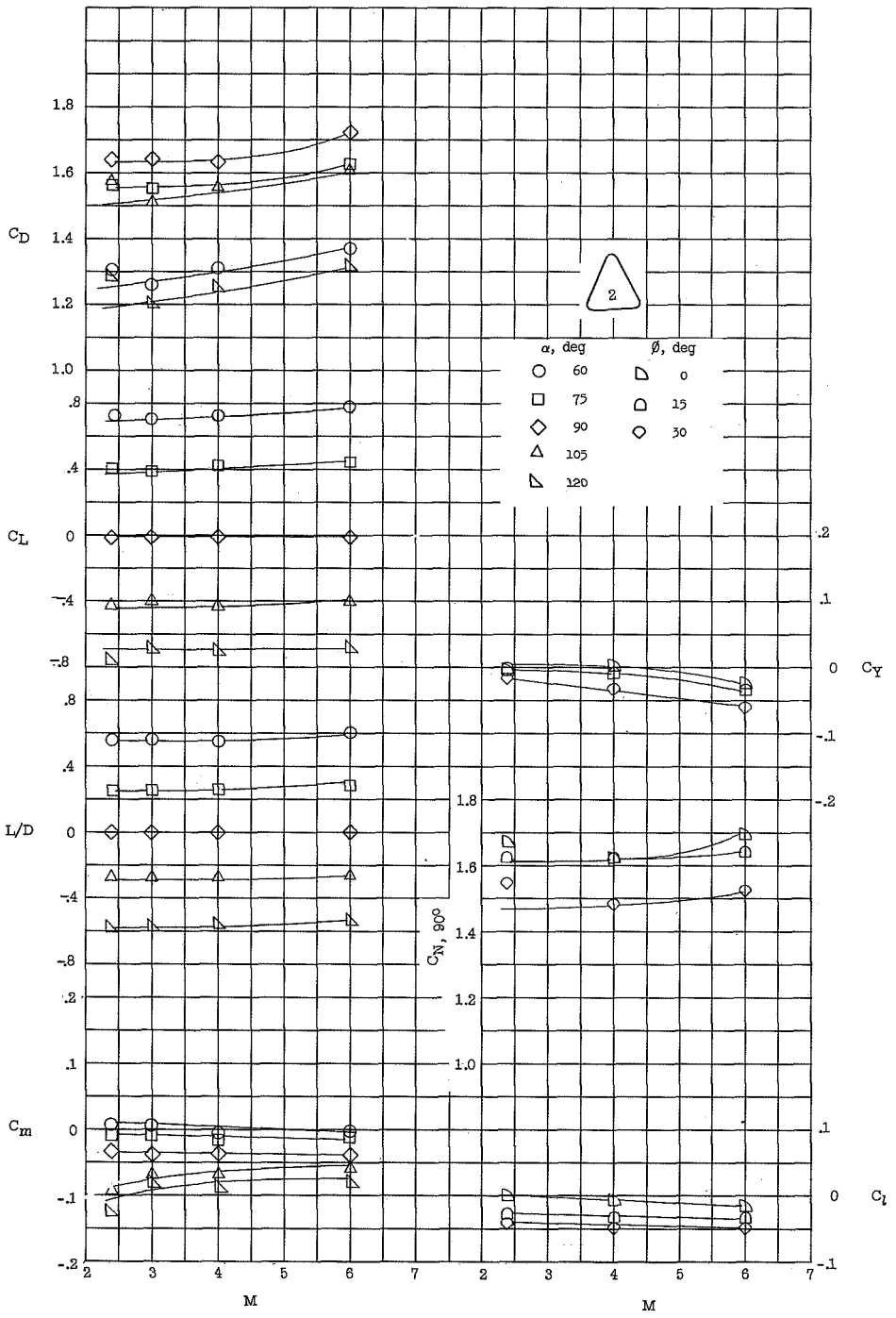

(g) Model 2.

Figure 17.- Continued.

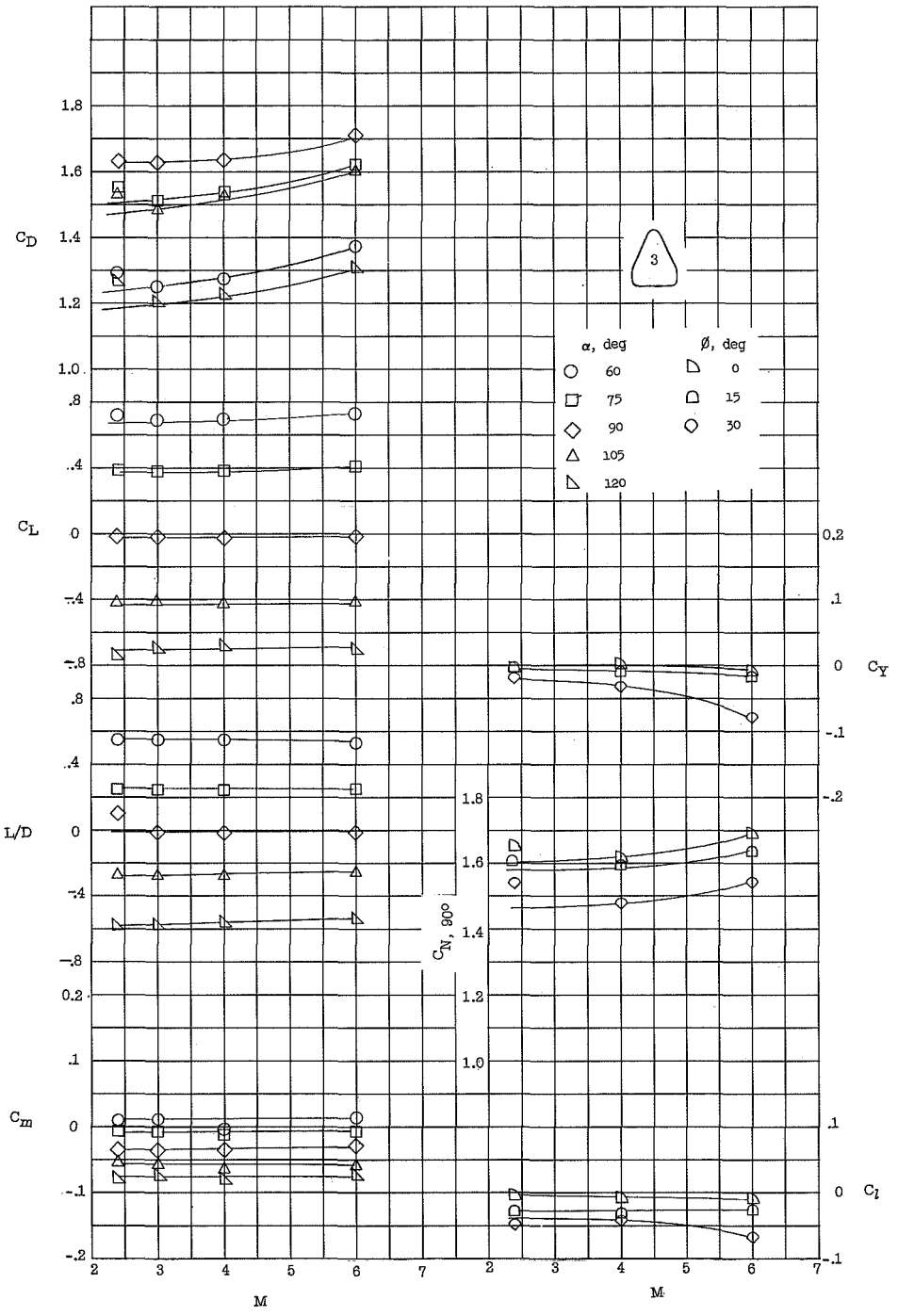

(h) Model 3.

Figure 17.- Continued.

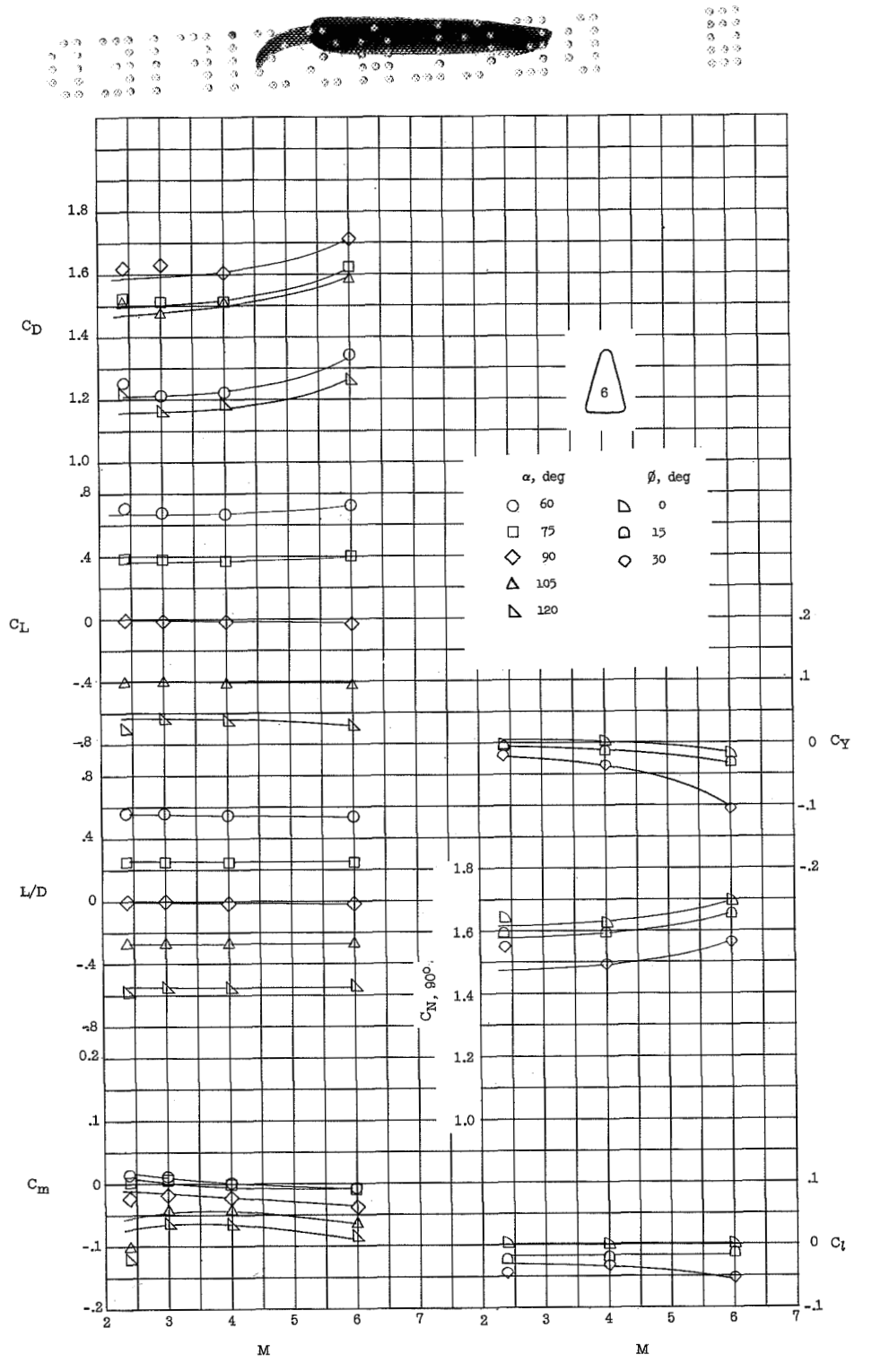

(i) Model 6.

Figure 17.- Continued.

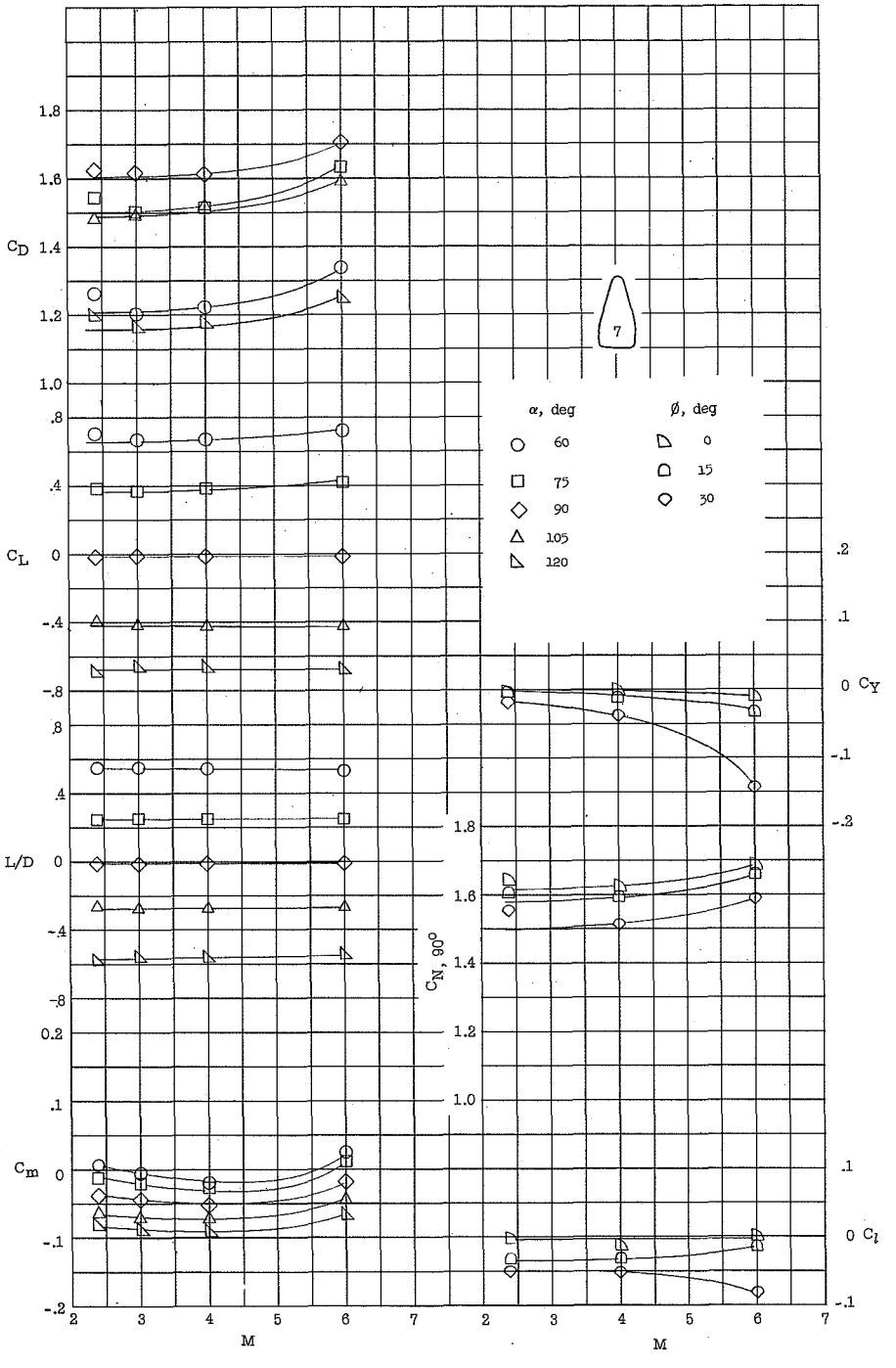

(j) Model 7.

Figure 17.- Continued.

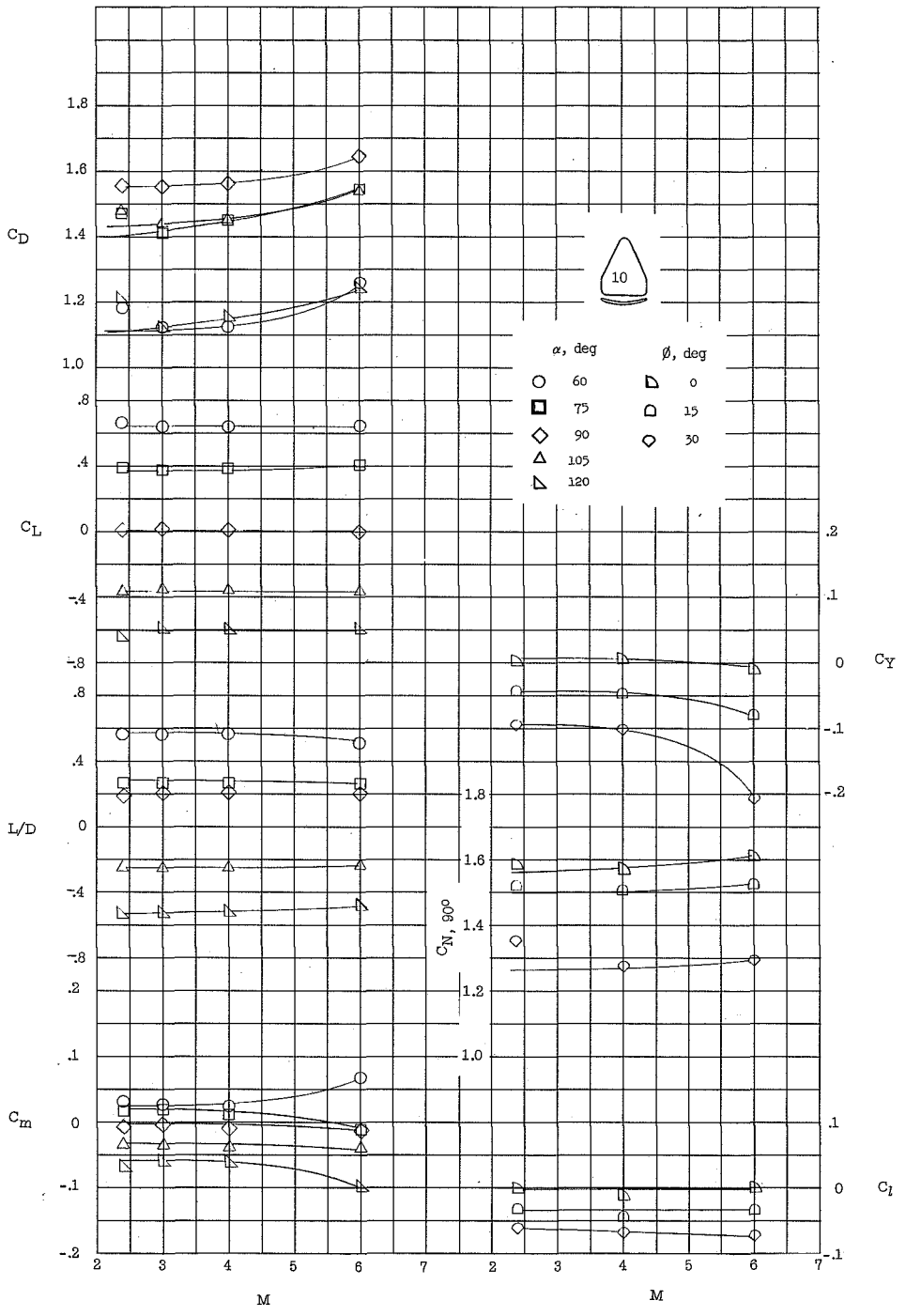

(k) Model 10.

Figure 17.- Concluded.